Bonding and Magnetism of $Fe_6-(C_6H_6)_m$, $m = 1, 2$

Israel Valencia, Alfredo Guevara-García, and Miguel Castro*

Departamento de Física y Química Teórica, DEPg, Facultad de Química, Universidad Nacional Autónoma de México, México D. F., C. P. 04510, México

Received: May 29, 2008; Revised Manuscript Received: April 20, 2009

The interactions of one and two benzene molecules with the superparamagnetic Fe_6 cluster were studied by means of gradient-corrected density functional theory. The ground state, GS, of bare Fe_6 presents a distorted octahedral structure with $2S = 20$; S is the total spin. For the calculated $2S = 16$ GS of the neutral $Fe_6-C_6H_6$ complex, as well as in the positive and negative ions both with $2S = 15$, the benzene unit is adsorbed on one axial Fe_a atom. The $2S = 14$ GS for $Fe_6-(C_6H_6)_2$ resembles a sandwich structure, with the metal Fe_6 cluster separating the benzene rings that are bonded symmetrically on the two axial sites of Fe_6. The binding is accounted for by electrostatic interactions and by $3d-\pi$ bonds, as revealed by the molecular orbitals. Though each C−Fe bond is weak, η^6 coordinations were indicated by the topology of the electronic density. The $3d-\pi$ bonding is reflected by the adiabatic ionization energies and electron affinities, which are smaller than those of bare Fe_6. The computed IR spectra show vibrational bands near those of bare benzene; some forbidden IR modes in benzene and in Fe_6 become IR active in $Fe_6-(C_6H_6)_{1,2}$. The results show a strong perturbation of the electronic structure of Fe_6. The decrease of its magnetic moment implies that the magnetic effects play an important role in the adsorption of benzene.

1. Introduction

Transition metal (TM) clusters present unusual structural, magnetic, and catalytic properties,[1] which finally depend on their electronic structure, different from those of the atom and bulk limits, that originate complicated metal−metal bonds and, in some cases, the formation of magnetic moments on the atomic sites. Particularly, small iron clusters, Fe_n, exhibit superparamagnetism because they have bigger moments than that of the bulk.[2,3] Very recently, using laser vaporization techniques,[4] the study for the adsorption of organic molecules on small TM clusters has been addressed.[5−7] In this way, neutral $Fe_n-(benzene)_m$ species were produced in the gas phase,[6,7] which were characterized mainly by mass spectrometry. Under high concentration of benzene, the mass spectrum revealed that the maximum m number of adsorbed moieties is smaller than n, allowing the proposal that $Fe_n-(benzene)_m$ has rice-ball structures consisting of an Fe_n cluster fully covered by benzene. The biggest observed system was Fe_7, being saturated with four benzenes, and was followed by Fe_6 which also adsorbs four ligands.[6,7] Such an amount of adsorbed moieties is consistent with the suggestion of rice-ball geometries for Fe_6 and Fe_7. However, relatively little experimental information is known on how the benzene molecules interact with iron clusters, specifically regarding the electronic and structural properties of the benzene adsorbed iron particles. In fact, rice-ball patterns were indicated for $Fe_n-(C_6H_6)_m$, but definitive experimental structural information is still elusive for these species. On the other hand, the coating of TM clusters with ligands may avoid their coalescence, mostly for iron, when one tries to link such particles, which is important for the design of new materials, with desired magnetic and/or catalytic properties, using TM clusters as building blocks. This implies also the study of the effects that ligands produce on the original attributes of the cluster, but little is known about this issue. Furthermore, the magnetic properties of complexes of TMs and polycyclic aromatic hydrocarbons (PAH), as extended systems of benzene, have raised considerable interest in recent years and motivated several theoretical and experimental studies.[8−10] Specifically, the IR properties of Fe−benzene compounds have been studied,[5] as well as those of PAH for astrophysical purposes.[11−14]

On the theoretical side, electronic structure calculations on TM clusters pose a considerable challenge, which is due to the abundance of low-lying electronic states, the possibility of multiple isomers, and the complicated nature of the TM atoms (occupying open 3d shells of short-range and close in energy, highly delocalized 4s orbitals). Even though multireference methods, where electronic wave functions are treated as multiconfigurational functions, are suitable and needed for the correct characterization of these kind of systems, their use is limited because of their expensive computational cost. These methods have been only applied to the study of TM dimers[15] or, regarding the present research, to the study of TM atoms interacting with a single benzene molecule.[16] The study of the TM ions bound to one benzene molecule has been realized at the modified coupled-pair (MCP) functional level.[17] More recently, Duncan and co-workers[5,18] have studied the TM−benzene ions with the use of the hybrid B3LYP functional;[19,20] they found good agreement with the MCP results as well as with experimental data.[5,18] It should be remarked that the study of TM clusters and of TM clusters interacting with molecules requires the use of functionals able to describe the complicated metal−metal interactions and the metal−ligand ones. In this regard, density functional theory (DFT), accounting for exchange correlation of many electron systems through the general gradient dependent approximation (GGA), for example the combination of the exchange functional proposed by Becke[21] and the one for correlation developed by Perdew and Wang,[22] jointly with the use of appropriate basis sets,[23] have proved to be

* To whom correspondence should be addressed. E-mail: castro@quetzal.pquim.unam.mx.

10.1021/jp811065w CCC: $40.75
Published on Web 05/07/2009

able to determine the ground state (GS) geometry and the electronic and energetic properties of TM systems or clusters presenting complicated metal−metal interactions.[24−27] In fact, DFT−GGA based methods allow the characterization of the GS properties for bigger clusters containing several TM atoms. As refs 24−27 show, DFT has succeeded in describing the electronic properties of magnetic TM clusters as well as the interaction of these particles with small molecules.

Specifically, Gutsev and Bauschlicher[24] have shown that the BPW91 method[21,22] is an appropriate GGA−DFT scheme for an accurate study of the structural, electronic, and energetic properties of small Fe_n, $n \leq 6$, clusters.[24] In their study, the requirement of more strict convergence criteria for the total energy and atomic forces, as well as the requirements of ultrafine grids, was pointed out.[24] The BPW91 approach and the 6311++G(2d,2p) orbital basis sets were employed, and the interactions of the superparamagnetic Fe_4 cluster with propane[25] and methane[26] were studied. More recently, we have also studied, with the BPW91/6311++G(2d,2p) method, the bonding and magnetic properties of the relatively small Fe_7 cluster interacting with a single benzene molecule.[27] In this last study, we have observed that calculations on $Fe_7-(C_6H_6)_1$ were quite computationally expensive, limiting the study of the adsorption process when two or more benzene moieties were considered.

The objective of this work is to study, by means of first principles all-electron calculations, performed with GGA−DFT, the interactions of benzene molecules with the magnetic Fe_6 cluster. It will be shown that the obtained results allow the determination of the geometry for the low-lying states that are produced from the interaction of the Fe_6 cluster with one and two benzene moieties, as well as the analysis of bond dissociation energies, ionization energies, and electron affinities. These structural and electronic results are useful for the study of the interactions between the 3d electrons of the cluster and the π cloud of benzene and to depict the type of bonding that occurs in the $Fe_6-(C_6H_6)_m$ species. We will also address the vibrational frequencies suffered by benzene in the adsorption process. The mono- and dibenzene complexes containing one TM atom have been studied extensively.[5] It will be shown that $Fe_6-(C_6H_6)_2$, resembling some features of ferrocene,[28,29] possesses unusual energetic and magnetic properties caused by the d−π bonding.

2. Methodology

The low-lying states of the Fe_6 cluster, benzene, and $Fe_6-(benzene)_m$ ($m = 1, 2$) complexes as well as those for the corresponding single positively and negatively charged species were determined with the aid of DFT all-electron calculations performed with the BPW91 functional,[21,22] which was used in concert with 6-311++G(2d,2p) basis sets (15s11p6d2f)/[10s7p4d2f] for Fe, (12s6p2d)/[5s4p2d] for C, and (6s2p)/[4s2p] for H.[23] The Gaussian-03 quantum chemistry software was used.[30] Here, also a strict convergence criterion was used for the total energy, minimized up to 10^{-8} au. Without imposed symmetry constraints and for different spin states, several candidate structures were fully optimized with a 10^{-5} au threshold for the root mean square (rms) force. An ultrafine grid was used for these steps and for the vibrational analysis, which was performed under the harmonic approximation for all optimized geometries. With this methodology, the regions of true minima states of the potential energy surface for each complex were searched. That is, the reported states in Figures 1−4 are true local minima because they have positive frequencies.

3. Results and Discussion

3a. Lowest Energy States Fe_6, Fe_6^+, and Fe_6^-. The GS of Fe_6 is a distorted octahedron of D_{2h} symmetry, shown in Figure 1, with a multiplicity $M = 2S + 1 = 21$; S is the total spin corresponding to a $^{21}A_u$ electronic state. The unpaired electrons form a magnetic moment of 20 bohr magnetons (μ_B) or 3.3 μ_B per atom. These results are in agreement with those reported by Gutsev and Bauschlicher,[24] Bobadova-Parvanova et al.,[31] as well as with our previous results.[32] Then, Fe_6 is a small cluster presenting high magnetic moment and geometry of relatively high symmetry. Experimentally, the Stern−Gerlach measurements are indicative of superparamagnetism in small iron clusters, as they have moments of $\cong$3.0 μ_B per atom, bigger than the bulk value, 2.2 μ_B.[2,3] The DFT results quoted above are consistent with such experimental findings. Table 1 contains some higher energy states of Fe_6. The average equilibrium bond length, R_{eq}, is also indicated, showing a shortening as the multiplicity decreases. The $M = 19$ state (3.0 μ_B/atom) lies nearest to the GS and may contribute, depending on temperature, on the measured moment. The other states may contribute negligibly as they lie at higher energies. Electron detachment from the $M = 21$ GS of Fe_6 yields, after full relaxation, an $M = 22$ GS for the Fe_6^+ ion, with an adiabatic ionization energy (IE) of 6.15 eV, which is near the experimental result, 5.96 ± 0.05 eV.[33] The GS geometry of Fe_6^+ is shown in Figure 2, as well as the highest occupied molecular orbital of minority spin, HOMO$^\downarrow$, from which the electron was deleted. Some higher energy states of Fe_6^+ are also indicated in Table 1. Assuming that one electron deletion from the excited states occurs either from the related HOMO$^\uparrow$, yielding an $M - 1$ state, or from HOMO$^\downarrow$, yielding an $M + 1$ state (M is the multiplicity of the parent neutral), and choosing the one of lowest energy, one finds that the IE for the higher energy states differs notably from the experiment; the departure increases as the energy of the state increases (see Table 1, in parentheses, the multiplicity of the produced Fe_6^+ ion is also indicated.). Attachment of one electron yields an $M = 20$ GS for Fe_6^-. Occupation was done on the lowest unoccupied molecular orbital, LUMO$^\downarrow$; see Figure 2. The estimated adiabatic electron affinity (AE), 1.61 eV, matches with the measured value, 1.58 ± 0.06 eV.[34] As is shown in Table 1, the estimated EAs for the higher energy states, assuming the M ± 1 rule quoted above, differ significantly from the experimental value. The importance of the spin effects in the accurate estimation of EAs and IEs for small iron clusters is exemplified by these results. The geometry of benzene is shown in Figure 1; its calculated IE, 9.08 eV, bigger than that of Fe_6, is close to the observed value, 9.24 eV.[35]

3b. Lowest Energy States of $Fe_6-(C_6H_6)$ and $Fe_6-(C_6H_6)_2$. The GS of $Fe_6-C_6H_6$ has C_{2v} symmetry with $M = 17$, yielding an $^{17}A_2$ electronic state, where the benzene molecule is adsorbed on one axial Fe_a atom, as shown in Figure 3. Note that the bonding of one axial iron atom with the carbon atoms of the benzene ring lengthens considerably the separations of Fe_a with the iron atoms in the equatorial plane; still, the structure of the whole Fe_6 cluster is preserved in this monobenzene compound. Concerning benzene, the bond lengths of the carbon atoms are slightly increased, from 1.40 to 1.42 Å, and the planarity is mostly maintained, since the dihedral angle in the ring is 1.1°. As shown in Table 2, the $M = 15$ state is quasidegenerate with the GS; other states lie at higher energies. Then, benzene adsorption reverses the order of the low-lying states of Fe_6, quenches the moment by about 4 μ_B, and forms a dipole moment of 2.37 Debyes (D). This last feature implies important electrostatic contributions in the Fe_6−benzene bonding.

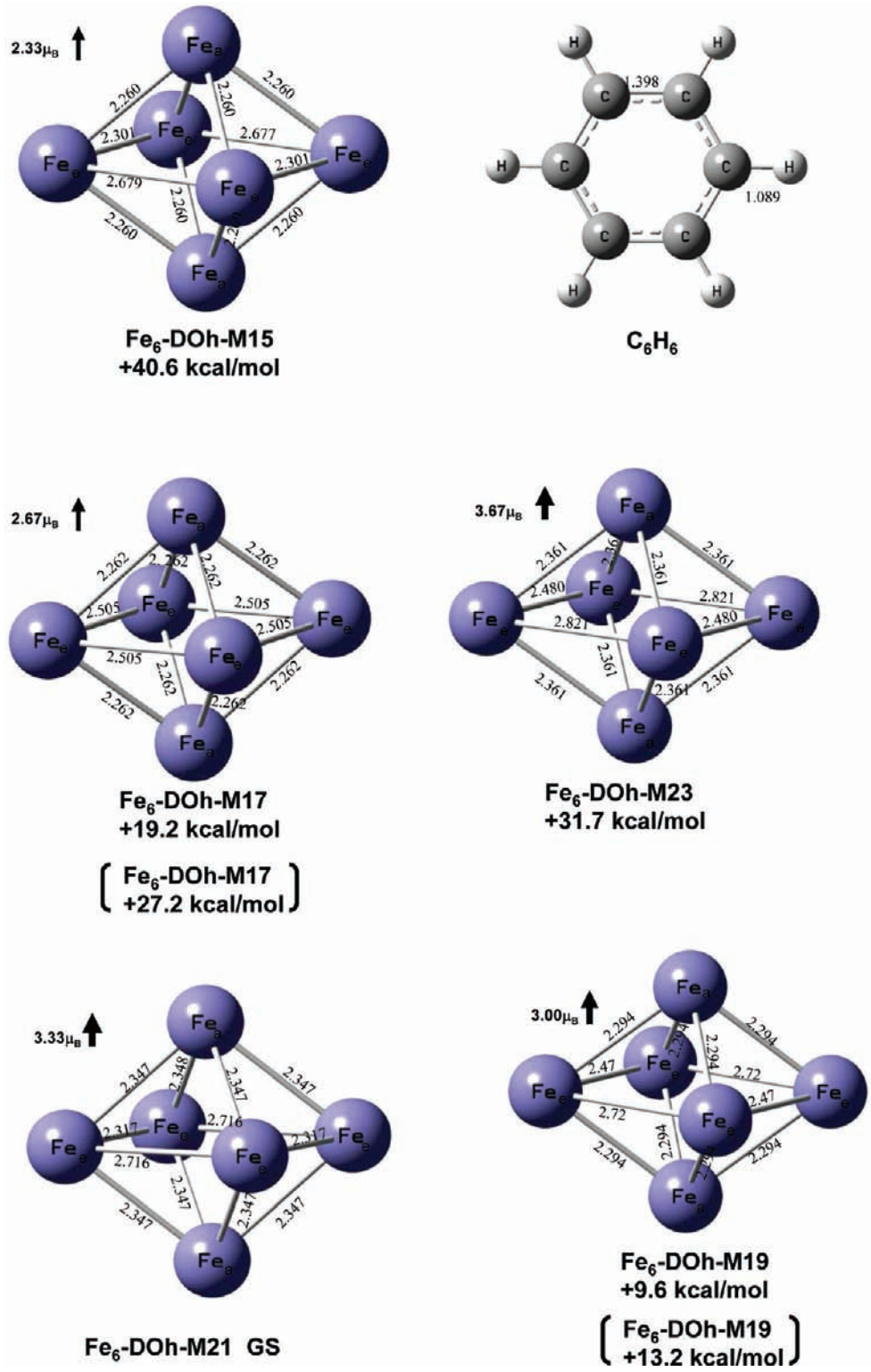

Figure 1. Lowest energy states for Fe_6. Bond lengths, in Å, and average magnetic moments per atom, in μ_B, are indicated. Also the calculated ground state for benzene is shown.

The GS of $Fe_6-(C_6H_6)_2$ has D_{2h} symmetry with $M = 15$, corresponding to the $^{15}B_{2\,g}$ electronic state, and the carbon atoms of the benzene molecules are bonded symmetrically, as depicted in Figure 4a, to the axial Fe atoms. These C−Fe η^6 coordinations produce a high compact structure, since the bond lengths among the equatorial Fe_e sites, aside from being equal to each other, 2.287 Å, are shorter than those of bare Fe_6, 2.716 and 2.317 Å. In Table 2 are reported other higher energy states of the axial isomers. The adiabatic IE and EA determined for the GSs of the complexes also are indicated there. Figure 4b shows the second lowest isomer, lying 5 kcal/mol over the GS, which comes from the bonding of one benzene to one axial Fe atom, and the other attached to one equatorial Fe site, producing, due to repulsion between the benzene units, a less symmetric and a more open geometry. Other axial−equatorial (AE) isomers lie at higher energies (see Table 2 and Figure 4b); they are distinguished by strong structural changes on the original geometry of the Fe_6 cluster. Then, these results show that the

TABLE 1: Lowest Energy States of the Fe_6, Fe_6^-, and Fe_6^+ Clusters, Computed with the BPW91/6-311++G(2d,2p) Method[a]

multiplicity	ΔE (kcal/mol)	R_{eq} (Å)	IE (eV)	ΔIE (eV)	EA (eV)	ΔEA (eV)
			Fe_6			
21	0.0	2.404	6.15 (22)[b]	0.19	1.61 (20)[c]	0.03
19	9.6	2.394	5.72 (20)[b]	0.24	2.18 (20)[c]	0.60
17	19.2	2.343	5.45 (18)[b]	0.51	2.40 (18)[c]	0.82
23	31.7	2.458				
15	40.6	2.336	5.35 (16)[b]	0.61	2.25 (16)[c]	0.67
			5.96 ± 0.05[d]		1.58 ± 0.06[e]	
			Fe_6^+			
22	0.00	2.429				
20	3.5	3.201				
18	11.3	3.170				
16	22.1	2.345				
14	29.3	2.304				
			Fe_6^-			
20	0.00	2.389				
18	8.8	2.366				
22	18.7	2.437				
16	24.9	2.311				

[a] Relative energies, ΔE, and average equilibrium bond lengths, R_{eq}, are indicated, as well as adiabatic ionization energies, IE, and electron affinities, EA, for each state. Also, the difference of the estimated IE and EA is shown, with respect to the experimental values. [b] Multiplicity of the Fe_6^+ cluster. [c] Multiplicity of the Fe_6^- cluster. [d] Experimental value from ref 33. [e] Experimental value from ref 34.

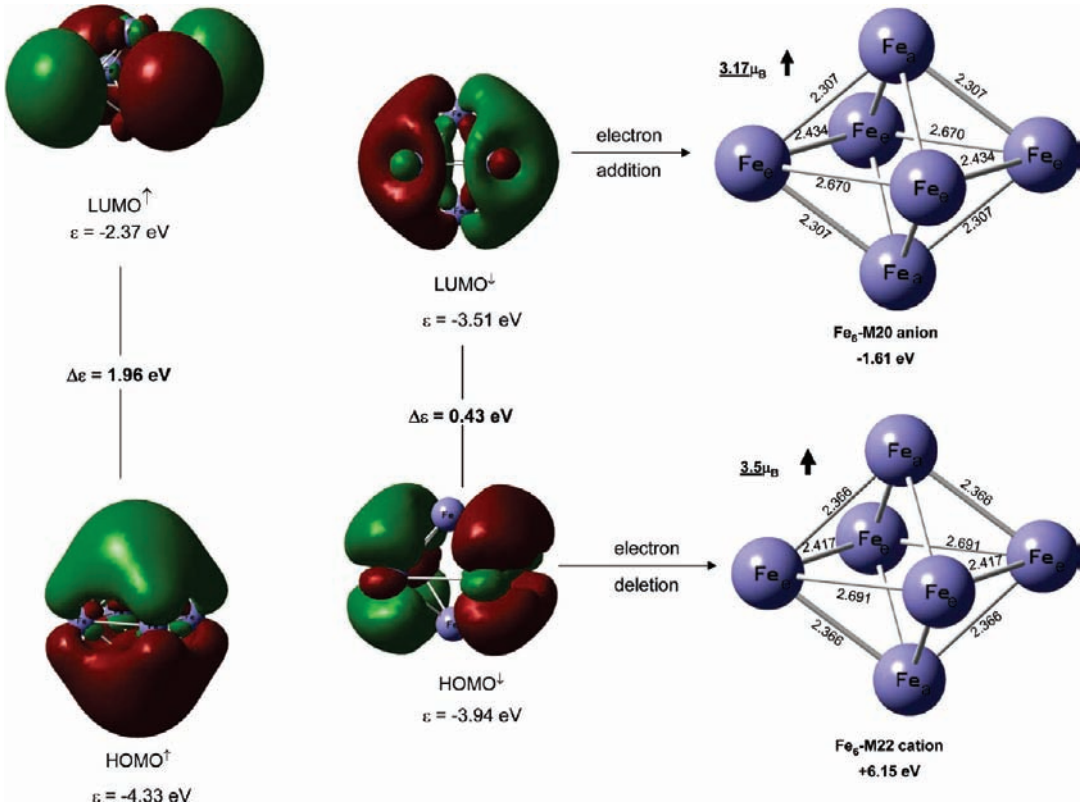

Figure 2. Contour plots for the HOMO and LUMO orbitals of the GS of neutral Fe_6. Also, the GS structures for the lowest energy states of the anion and cation are shown.

GS geometry of the Fe_6−dibenzene complex resembles some kind of sandwich geometry, with the metal Fe_6 unit separating the two benzene rings. Consistently, a dipole moment equal to zero was obtained for this symmetric structure. On the other hand, Zheng et al.[36] have pointed out the possibility of sandwich structures for the dibenzene complexes of the Fe_2, Fe_3, and Fe_4 clusters. The present results show how the Fe_6 cluster adsorbs two benzene molecules producing such kind of structures.[36] Thus, adsorption of two benzene moieties quenches the moment, by 6 μ_B, more strongly than one adsorption. For low temperatures, near 0 K, a value of 2.3 μ_B per atom is predicted for $Fe_6-(C_6H_6)_2$. These results agree with the experimental finding that the moments of small magnetic cobalt clusters are reduced considerably by the adsorption of benzene.[37]

3c. Bonding Molecular Orbitals of $Fe_6-C_6H_6$ and $Fe_6-(C_6H_6)_2$. In $Fe_6-C_6H_6$ and $Fe_6-(C_6H_6)_2$, the C−Fe contacts, 2.106−2.118 and 2.133−2.138 Å, respectively, are a bit longer than those of ferrocene,[38] 2.045 Å, prototypical of C−Fe covalent bonds, but they are shorter than the sum of the van der Waals radii of C (1.7 Å) and Fe (1.9 Å), suggesting C−Fe bonding, which, aside from the electrostatic attractive interactions quoted above, is due to the covalent bond formation arising

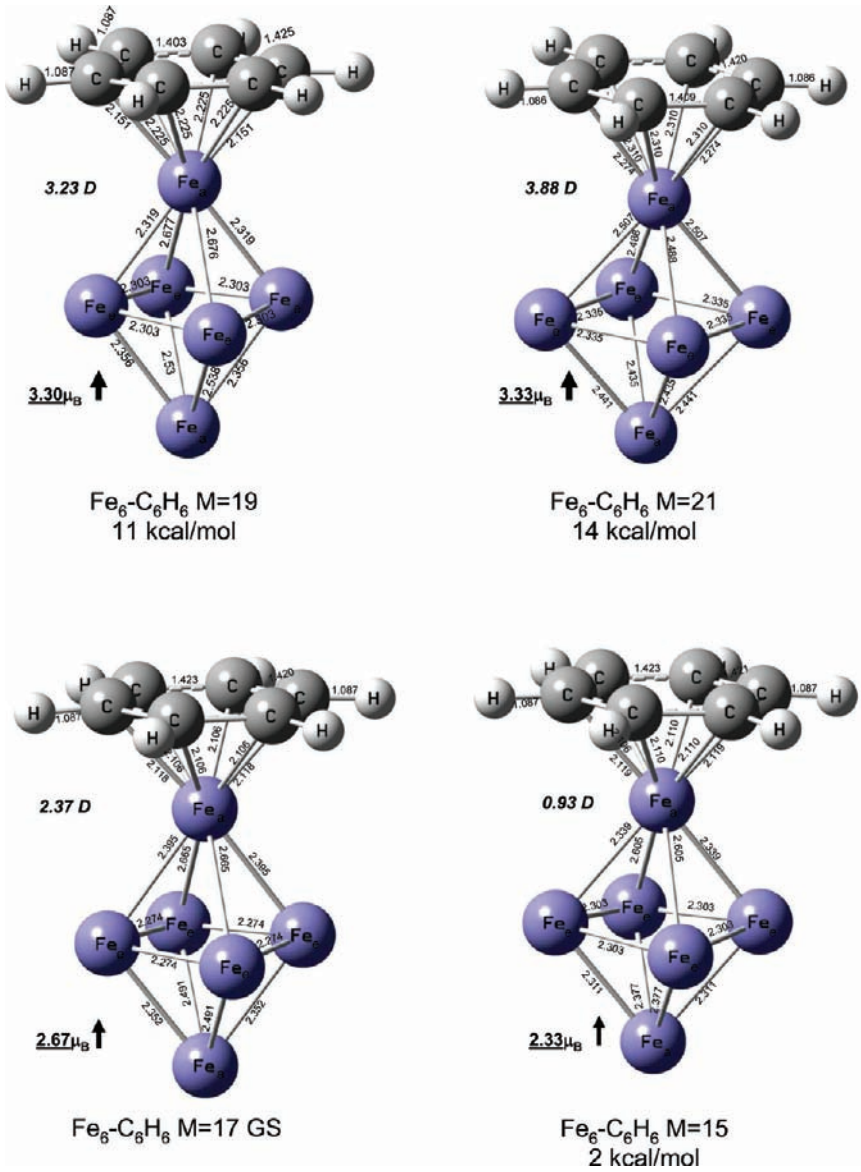

Figure 3. Bond lengths, in Å, average magnetic moments per atom, in μ_B, and dipole moments, in Debyes, for the lowest energy states of $Fe_6-C_6H_6$.

from the orbitals, mainly of 3d type, of the cluster and the π cloud of benzene, as will be described below.

The C−Fe bond formation was analyzed by the contour plots of the molecular orbitals (MO), of majority spin, of the $Fe_6-(C_6H_6)_2$ GS. Those MOs with bond signatures between the 3d electrons of the Fe_a sites and the π cloud of benzene are shown in Figure 5. Specifically, HOMO shows weak C−Fe bonding, while HOMO−7 and HOMO−12 indicates clear bond formation between the 3d orbitals of the Fe_a atoms and the π electrons. In HOMO−11, both axial and equatorial atoms are involved in the $Fe_6-C_6H_6$ bond formation, and in HOMO−39, apart from a markedly C−Fe_a bonding, the symmetric π MO of benzene remains delocalized around the ring. Other MOs (see Figure 6) are polarized from the Fe_a sites toward the Fe_e atoms, signifying transference of electrons into the equatorial plane. Some electronic delocalization around that plane is depicted by HOMO−3, HOMO−5, and HOMO−23. These MOs show bonding behavior in the square, and they produce a shortening of the Fe_e-Fe_e bond lengths. In Figure 1 of the Supporting Information section, the MOs of spin down showing C−Fe bonding are reported; those with Fe_a-Fe_e polarization and delocalization in the equatorial plane are also reported there in Figure 2. As shown in panels a and b of Figure 3 of the Supporting Information, the formations of 3d−π bonds are also accomplished in $Fe_6-C_6H_6$. This kind of bonding and the electrostatic contributions accounts for the relatively short, 2.106−2.118 Å, C−Fe contacts of $Fe_6-C_6H_6$.

Both, LUMO and HOMO of $Fe_6-(C_6H6)_{1,2}$ have signatures on the benzene units (see Figure 5 and Figure 3a of the Supporting Information), and their gaps, 0.79 and 0.74 eV, are notably smaller than that of bare benzene, 5 eV, suggesting an increase of the softness for the adsorbed benzene.

As mentioned, some MOs of $Fe_6-(C_6H_6)_2$ show bonding behavior in the square ring, producing a shortening of the Fe_e-Fe_e distances. Effectively, the Fe−Fe bond lengths in the equatorial plane have the same value, 2.274 Å for $Fe_6-C_6H_6$ and 2.287 Å for $Fe_6-(C_6H_6)_2$, and they are shorter than the distances in the rectangular plane of the GS of Fe_6; they also are shorter than the average for the $M = 17$ (2.57 Å) and $M = 15$ (2.49 Å) states of Fe_6. These results are indicative of an increase of the metal−metal bonding in the square planes of $Fe_6-C_6H_6$ and of $Fe_6-(C_6H_6)_2$. Besides, the whole Fe−Fe

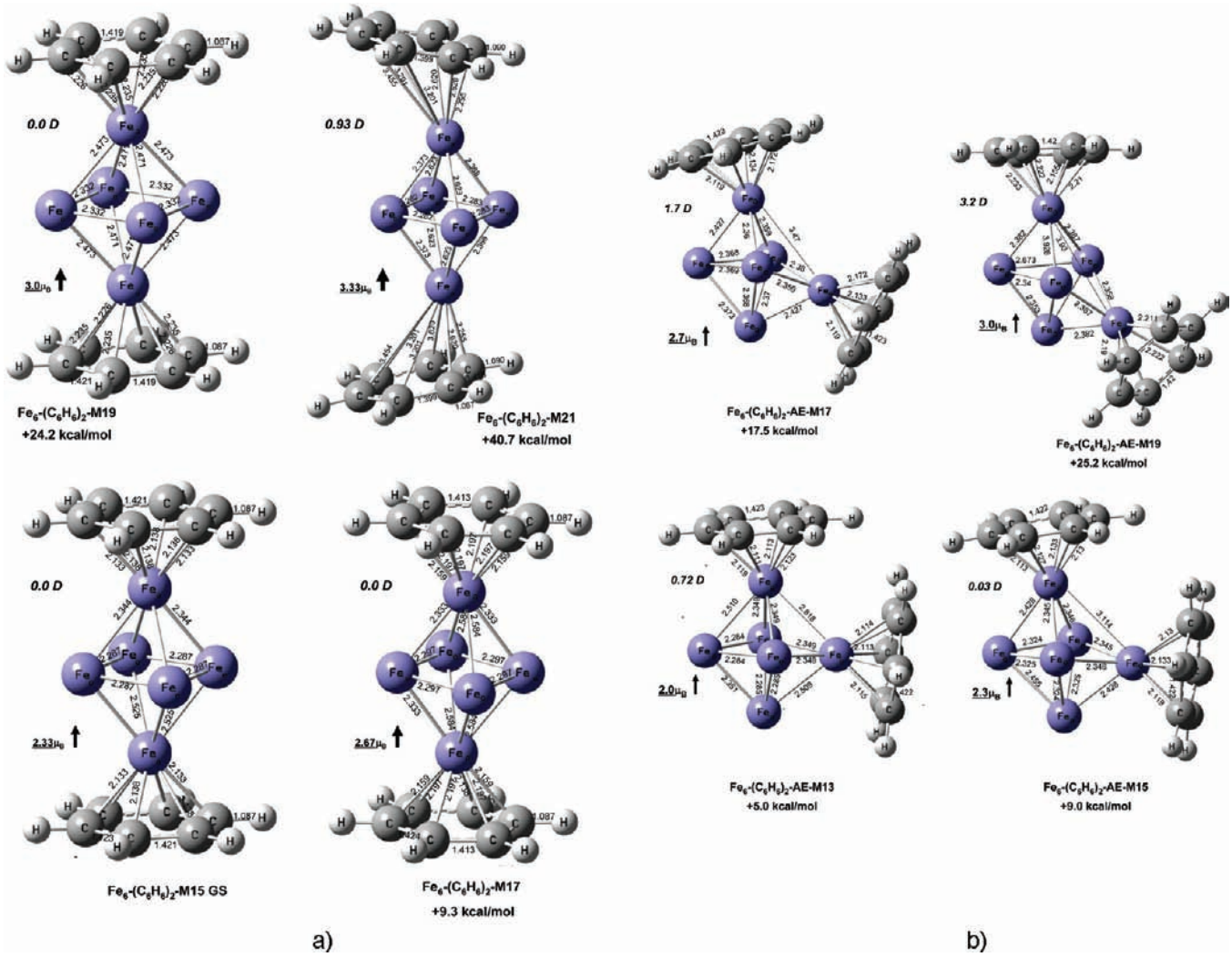

Figure 4. (a) Bond lengths, in Å, average magnetic moments per atom, in μ_B, and dipole moments, in Debyes, for the lowest energy states of the axial−axial isomers of $Fe_6-(C_6H_6)_2$. (b) Bond lengths, in Å, average magnetic moments per atom, in μ_B, and dipole moments, in Debyes, for the low-lying states of the axial−equatorial isomers of $Fe_6-(C_6H_6)_2$.

TABLE 2: Lowest Energy States of the $[Fe_6-(C_6H_6)_m]$, m =1, 2 Complexes[a]

multiplicity	ΔE (kcal/mol)	IE (eV)	EA (eV)
	$Fe_6-C_6H_6$		
17	0.0	5.31 (16)[b]	1.44 (16)[c]
15	2.0		
19	11		
21	14		
	$Fe_6-(C_6H_6)_2$		
	axial isomers		
15	0.00	4.90 (16)[b]	0.86 (16)[c]
17	9.3		
19	24.2		
21	40.7		
	axial−equatorial isomers		
13	5.0		
15	9.0		
17	17.5		
19	25.2		

[a] Relative energies, adiabatic ionization energies, and electron affinities are indicated. [b] Multiplicity of the lowest energy state of $[Fe_6-(C_6H_6)_m]^+$, $m = 1$ or 2. [c] Multiplicity of the lowest energy state of $[Fe_6-(C_6H_6)_m]^-$, $m = 1$ or 2.

average distance (2.385 Å) of Fe_6 in $Fe_6-(C_6H_6)_2$ is somewhat shorter than that of free Fe_6, 2.404 Å. Thus, aside from the quenching of the magnetization, a shrinking of Fe_6 is produced in the dibenzene complex.

Up to here, the results show that the Fe_6−benzene bonding is due to the electrostatic contributions and to the covalent bonds arising from the 3d orbitals and the π cloud. Below, it will be determined if each carbon atom effectively is bonded to the Fe_a sites, yielding η^6 coordinations or lower ones, and the strength of the Fe−C bonds, expected to be weak, since a small lengthening, ≅0.02 Å, was found for the C−C bond lengths in $Fe_6-(C_6H_6)_{1,2}$.

The $Fe_6-C_6H_6$ and $Fe_6-(C_6H_6)_2$ GSs are true minima on the potential energy surface, where all atomic forces are zero, because full optimization produces positive frequencies. For such equilibrium structures, the theory of atoms in molecules (AIM) has proved to be useful for depicting the bond formation through the topological analysis of the electronic density, ρ, and the Laplacian, $\nabla^2\rho$.[39] Taken as input the GS wave function of $Fe_6-C_6H_6$ and $Fe_6-(C_6H_6)_2$, AIM[40] defines bond critical points (BCP) for the C−Fe contacts as well as gradient paths originating at BCP and terminating at the C and Fe nucleus, which is the topological criteria[41] for a bond formation between the C and Fe centers. Figure 7 contains the AIM results for $Fe_6-(C_6H_6)_2$; a similar picture was found for $Fe_6-C_6H_6$. Consequently, these C−Fe bonds originate the formation of

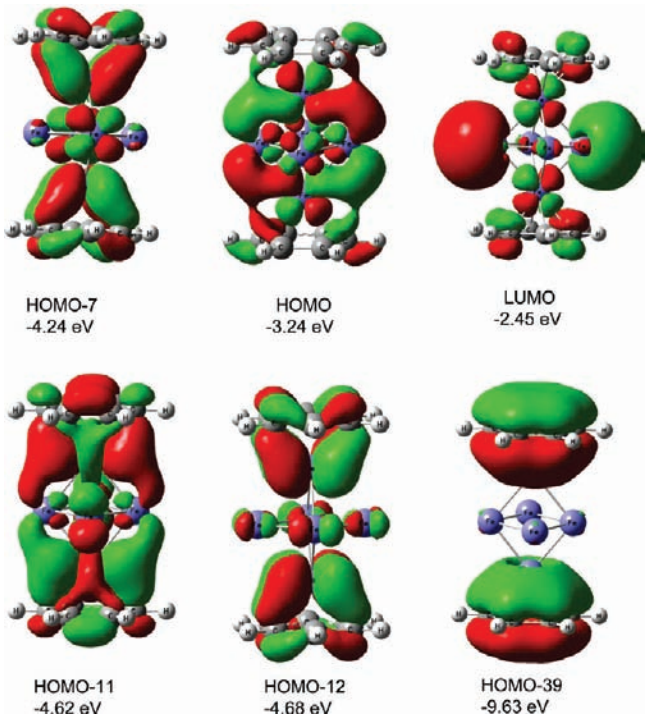

Figure 5. Contour plots for the C−Fe_a bonding molecular orbitals of the $Fe_6-(C_6H_6)_2$ GS.

Fe−C−C rings, for which AIM yields the related ring critical points, RCP. Critical points and C−Fe bond paths are shown in Figure 7. Then, C−Fe η^6 coordinations occur in the mono- and dibenzene complexes. Note that the positive $\nabla^2\rho$ values show a locally depleted electronic density on the C−Fe bonds. For $Fe_6-(C_6H_6)_2$, AIM reveals the formation of twelve Fe−Fe bonds in the compact Fe_6 region, where apart from the BCPs and RCPs, a cage critical point, CCP, also appears. These AIM results are consistent with the analysis of the MOs discussed above, which indicate, with respect to the GS of the free Fe_6 cluster, an increase of the bonding in the Fe_6 region of the $Fe_6-(C_6H_6)_2$ complex, accounting for the shortening of the average Fe−Fe distance of the coated cluster. Also, some MOs showed electron delocalization in the equatorial plane of the Fe_6 region of the complex. Consistently, the $\nabla^2\rho$ values indicate a lesser concentrated electronic density for the Fe_e-Fe_e bonds in the equatorial plane than for the axial−equatorial iron bonds; see Figure 7. See also Figure 4, for $Fe_6-C_6H_6$, in the Supporting Information.

3d. Ionization Energies, Electron Affinities, and Bond Dissociation Energies. Electron detachment was also considered. After a full, structural, and electronic relaxation, an $M = 16$ GS was found for $[Fe_6-(C_6H_6)]^+$, with an adiabatic IE of 5.31 eV. The $[Fe_6-(C_6H_6)_2]^+$ ion presents also $M = 16$ but with a more diminished IE, of 4.90 eV. These low ionization energies, which are smaller than those of bare Fe_6 (6.15 eV) and benzene (9.08 eV), are clear signatures of d−π interactions.[7] They also suggest that the electron is mainly deleted from the Fe_6 moiety. This is just the case for $Fe_6-(C_6H_6)_2$ where the electron is removed from the HOMO$^{\downarrow}$, reported in Figure 1 of the Supporting Information, which shows strong contributions on the Fe_6 region, mostly on the equatorial plane. Also, note that the IE decreases as more benzene moieties are added. The IEs of $Fe_6-(C_6H_6)_m$ ($m = 1, 2$) have not yet been measured, but the determined IEs for $Fe-(C_6H_6)_m$ ($m = 1, 2$), >6.42 and 5.18 ± 5 eV,[7] respectively, are clearly smaller than the IE for the bare Fe atom, 7.87 eV, and they also decrease from $m = 1$ to $m = 2$. Our results for $Fe_6-(C_6H_6)_{1,2}$ follow this experimental tendency. (We have obtained an IE of 6.44 eV for $Fe-C_6H_6$, which is in line with the measurements of Kurikawa et al.,[7] indicating a value greater than 6.42 eV.) The difference of IE for Fe_6 and $Fe-(C_6H_6)_2$, 1.25 eV, suggest significant delocalization of the most external electrons of Fe_6 through the $Fe_6-(C_6H_6)_2$ adduct, which is accomplished through the network of the 3d−π bonds. It is interesting to compare these findings with the results of Senapati et al.[8] for iron atoms supported on coronene ($C_{24}H_{12}$), a PAH compound. Specifically, for Fe−coronene and Fe_2−coronene, the adiabatic IEs, 5.51 and 5.54 eV, respectively, are near to the values quoted above, 5.31 and 4.90 eV for $(Fe_6-C_6H_6)_{1,2}$. They also are smaller than those of the separated species, Fe (7.64 eV), Fe_2 (6.55 eV), and coronene (7.19 eV), with the peculiarity that the IE of Fe−coronene is closer to that of coronene, while for Fe_2−coronene it is closer to Fe_2, signifying that in the former case the electron is removed from coronene, whereas in Fe_2−coronene, the detachment is done from the Fe_2 cluster.[8] This last behavior is similar to our present results for the $Fe_6-C_6H_6$ complexes, on which electron deletion mainly occurs from Fe_6.

Moreover, addition of one electron gives the $[Fe_6-C_6H_6]^-$ and $[Fe_6-(C_6H_6)_2]^-$ ions, both with $M = 16$ GSs and with smaller adiabatic electron affinities, 1.44 and 0.86 eV, respectively, than that of Fe_6, 1.61 eV; note the larger decrease for the $Fe_6-(C_6H_6)_2$ adduct. (It should be mentioned that we have obtained an adiabatic EA of 0.47 eV for $Fe-C_6H_6$, which is in close agreement with the experimental value, 0.46 ± 0.1 eV, determined recently by Zheng et al. for this isolated complex in the gas phase, by means of negative ion photoelectron spectroscopy techniques.[36]) This and the reduction of the IE confirm that the most external electrons of the neutral and charged $[Fe_6-(C_6H_6)_m]$ ($m = 1, 2$)complexes are less bonded than those of the bare Fe_6 cluster. Indeed, the HOMO of $[Fe_6-(C_6H_6)_2]^-$ is very similar to the LUMO$^{\uparrow}$ of the neutral, lying over the whole adduct, with huge contributions on the equatorial plane of Fe_6; see Figure 5.

When one subtracts the GS energies of Fe_6 and C_6H_6 from that of $Fe_6-(C_6H_6)_2$, a bond dissociation energy (BDE), including zero point energy corrections, of 47.9 kcal/mol was obtained, or ≅24 kcal/mol per benzene, yielding a bond strength of about 4 kcal/mol for each C−Fe bond. Similarly, the calculated BDE for $Fe_6-C_6H_6$ is 19.9 kcal/mol or 0.86 eV. The BDEs for the neutral and charged $Fe_6-(C_6H_6)_{1,2}$ complexes are reported in Table 3. Besides, with respect to the $Fe_6-C_6H_6$ GS, the BDE for the second benzene is 28.1 kcal/mol. Thus, in a sequential addition, the BDE for the second step shows an enhancement, which is indicative of a bigger stability for the $Fe_6-(C_6H_6)_2$ adduct. These results give insight that the structures of $Fe_n(C_6H_6)_m$, as inferred from spectroscopic and chemical probe studies, consist of an Fe_n cluster surrounded by a strongly adsorbed layer of benzene molecules.[6,7] Moreover, on experimental grounds, the BDE of $Fe-C_6H_6$ is estimated to be greater than 16.1 kcal/mol; our values are consistent with this finding for a single Fe atom[7,42,43] and with the BDE of benzene, 24.7 kcal/mol, on an infinite Fe(100) surface.[44] On the other hand, Simon and Joblin have studied, with DFT methods, the interaction of a single iron atom with naphthalene ($C_{10}H_8$), pyrene ($C_{16}H_{10}$), and corenene, which are of interest for astrophysics.[12] They found that the BDEs for neutral Fe−naphthalene (0.64 eV), Fe−pyrene (0.68 eV), and Fe−coronene (0.62 eV) hardly change with the PAH compound. A standard value of 0.6 eV or 13.8 kcal/mol was indicated for the binding energy between iron and neutral PAH, which is relatively close to the BDE for $Fe-C_6H_6$ mentioned above.

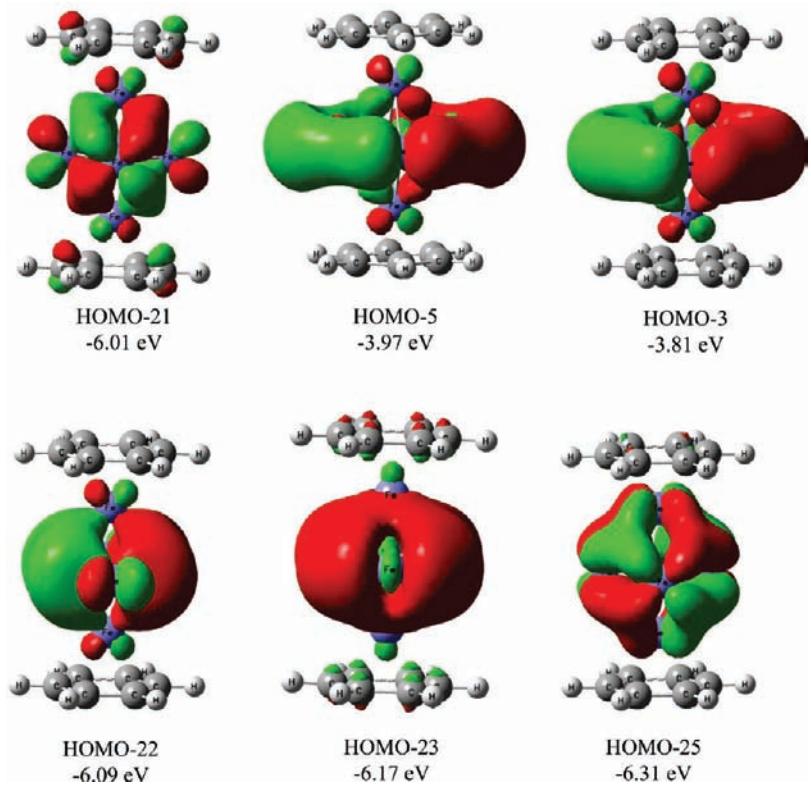

Figure 6. Contour plots for the molecular orbitals of $Fe_6-(C_6H_6)_2$. They show polarization from the axial toward the equatorial iron atoms and delocalization in the equatorial plane.

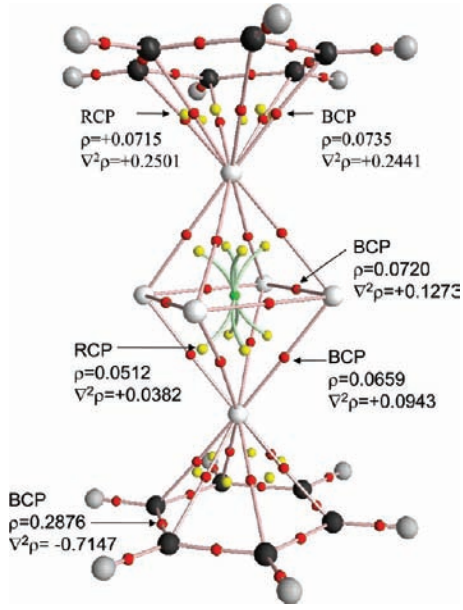

Figure 7. Molecular graph for the GS of $Fe_6-(C_6H_6)_2$. The density (ρ), in e au^{-3}, and Laplacians ($\nabla^2\rho$), in e au^{-5}, for the BCPs of the C−Fe and Fe−Fe contacts and the RCPs of the Fe−C−C and Fe−Fe−Fe rings are indicated.

Furthermore, a BDE of 24.7 kcal/mol has been estimated for Fe_2−coronene, producing Fe_2 and coronene,[8] which is markedly close to our results for the $Fe_6-(C_6H_6)_{1,2}$ complexes.

Assuming an Fe_6^+ + benzene dissociation channel, which is reasonable because the IE of Fe_6 is smaller than that of benzene, an adiabatic BDE of 1.68 eV or 38.8 kcal/mol was obtained for $[Fe_6-(C_6H_6)]^+$. Likewise, a BDE of 3.32 eV or 76.6 kcal/mol (1.66 eV or 38.3 kcal/mol per benzene) was found for $[Fe_6-(C_6H_6)_2]^+$. These binding energies are bigger than those

TABLE 3: Adiabatic Bond Dissociation Energies per Benzene Molecule, for the Neutral and Charged Species of the $[Fe_6-(C_6H_6)_m]$ ($m = 1$ and 2) Complexes

complex	products	BDE (kcal/mol)
$Fe_6-C_6H_6$	$F_6 + C_6H_6$	19.9
$Fe_6-(C_6H_6)_2$	$Fe_6 + 2C_6H_6$	24.0
$[Fe_6-C_6H_6]^+$	$Fe_6^+ + C_6H_6$	38.8
$[Fe_6-(C_6H_6)_2]^+$	$Fe_6^+ + 2C_6H_6$	38.3
$[Fe_6-C_6H_6]^-$	$Fe_6^- + C_6H_6$	16.9
$[Fe_6-(C_6H_6)_2]^-$	$Fe_6^- + 2C_6H_6$	16.2

of the neutrals and are accounted for by an increase of the electrostatic contributions. That is, the benzene moieties are more strongly adsorbed on Fe_6^+ than on Fe_6. Experimentally,[42] the determined BDEs for $[Fe-(C_6H_6)_m]^+$ ($m = 1$ and 2) are equal to 2.15 ± 0.10 and 1.94 ± 0.17 eV, respectively; they are close to each other, with the latter slightly smaller. Our results for Fe_6 closely follow this energetic behavior. As expected, the binding energy between the Fe_6^+ cluster and the benzene molecule is lower than the corresponding energy for Fe^+. This is because of the Fe−Fe bonding interactions that the axial Fe atom, coordinated directly to benzene, presents in the $[Fe_6-(C_6H_6)]^+$ complex. Due to the metal−metal bonding, the interaction of TM clusters with benzene produce bonding patterns different from those observed in single TM ions. These results should be compared with the BDEs for $[Fe-naphthalene]^+$ (2.77 eV), $[Fe-pyrene]^+$ (2.60 eV), and $[Fe-coronene]^+$ (2.59 eV), which are significantly bigger than the BDE of $[Fe_6-(C_6H_6)_{1,2}]^+$, 1.68−1.66 eV. This difference could be partially accounted for by the fact that in Fe−PAH the electron is deleted from the PAH moieties, because these bare PAH molecules have smaller IEs than the Fe atom, while in $Fe_6-C_6H_6$ it is deleted from the Fe_6 cluster. In fact, for the Fe_2^+ + coronene dissociation channel, Senapati et al.[8] have determined a BDE of 2.08 eV for $[Fe_2-coronene]^+$, which is

more closer to our BDE results for $[Fe_6-(C_6H_6)_{1,2}]$, although other dissociation paths were found to be more favorable for $[Fe_2-\text{coronene}]^+$.

For the $[Fe_6-C_6H_6]^-$ ion, an adiabatic BDE of 16.9 kcal/mol was obtained under the assumption of an Fe_6^- + benzene dissociation, which is in line with the well-known feature that benzene does not bind an additional electron. In the same way, a BDE of 1.41 eV or 32.42 kcal/mol (0.70 eV or 16.21 kcal/mol per benzene) was found for $[Fe_6-(C_6H_6)_2]^-$, dissociating into Fe_6^- + 2 benzene, while dissociation into $[Fe_6-C_6H_6]^-$ + benzene yields a considerable smaller BDE, 0.67 eV or 15.5 kcal/mol. These binding energies are smaller than those of the neutrals and cations. Hence, on the $[Fe_6-(C_6H_6)_{1,2}]^-$ complexes the benzene molecules are less strongly adsorbed on the Fe_6 core, which is accounted for by the repulsion of Fe_6^- with the π cloud.

Then, in $Fe_6-(C_6H_6)_m$ (m = 1, 2), there is a considerable relaxation of the electronic structure of Fe_6, as shown by the strong changes of the IEs, EAs, and magnetic moments. As shown above, the adsorption of benzene notably quenches the magnetization of Fe_6, 4 μ_B for m = 1 and 6 μ_B for m = 2. The coating of the cluster switch on a spin paired process, which apart from the C−Fe bond formation also produces an increase of the metal−metal bonding. The shortening of the Fe−Fe distances found for m = 2 indicate that such bonding truly increases. The decrease of the atomic magnetic moments is closely connected with the reduction of the repulsive interactions between the 3d electrons of Fe_6 and the π cloud of benzene. Smaller moments on the Fe atoms mean that there are smaller amounts of 3d electrons at those sites, resulting in a reduction of the repulsion with the π electrons. These results agree in that the moment of an Fe atom is reduced from 4 to 2 μ_B when adsorbed in benzene.[43,45] Thus, magnetic effects are crucial for the bonding of C_6H_6 with Fe_6.

3e. Vibrational Analysis: Fe_6, C_6H_6, and $Fe_6-C_6H_6$. The computed frequencies for the GS of Fe_6 fall in the low-frequency 54−336 cm^{-1} region, and those for benzene in the gas phase are contained within 394−3132 cm^{-1}. Thus, the gaps of the frequencies for the free Fe_6 and benzene species do not overlap each other. The estimated IR spectra for the Fe_6, C_6H_6, and $Fe_6-C_6H_6$ species are shown in Figure 8. The main IR-active bands of benzene were found at 661, 1034, and 1472 cm^{-1}, they are for the ν_{11} (out-of-plane C−H bend), ν_{18} (in-plane C−H bend), and ν_{19} (in-plane carbon ring distortion) vibrational resonances, respectively. These BPW91 results are only slightly smaller than the experimental values: 673, 1038, and 1486 cm^{-1}.[46] Another IR-active band for the asymmetric C−H stretching mode was located at 3121 cm^{-1}; see Figure 8b. Close to this mode is positioned the fully symmetric C−H stretching mode, which is IR inactive and reaches the highest frequency, 3132 cm^{-1}, for the bare benzene molecule. The complete list of the calculated vibrational frequencies for benzene is shown in Table 4, together with the reported experimental values; intensities, in km/mol, are also indicated. Overall, the theoretical estimations show relatively small errors, the biggest departures, of 3.9%, occur for the in-plane C−H bending and the in-plane carbon ring distortions. Regarding Fe_6, its main active IR bands, shown in Figure 8a, were found at 245, 254, and 300 cm^{-1}, with quite small intensities of 1.3, 3.6, and 1.6 km/mol, respectively. These frequencies account for asymmetric stretching modes. Another two vibrations, lying at 54 and 147 cm^{-1}, have negligible contributions to the IR spectrum. It should be mentioned that the full symmetric stretching mode of Fe_6, which is IR inactive, is situated at the top value, 336.3 cm^{-1}, of the vibrational frequencies for this isolated cluster.

For the M = 17 GS of $Fe_6-C_6H_6$, the frequencies fall in the 11−3142 cm^{-1} range. Two main features emerges from its IR spectrum: (1) it presents vibrational bands near those of the free benzene molecule, and (2) some forbidden IR modes of benzene become IR active in the reduced symmetry of the complex, which has a dipole moment of 2.37 D. These kinds of frequencies are reported in Table 4 and also are indicated in Figure 8c. Specifically, the strongest resonance is for the out-of-plane C−H bend mode lying at a higher value, 775 cm^{-1}, than in bare benzene; the shift to the blue is of 114 cm^{-1}. The notorious bands at 833−838 cm^{-1}, IR inactive in free benzene, present also this kind of C−H bend mode; they become IR active in the complex with small shifts in their frequencies, of 2.8 and 6.9 cm^{-1}. Also the symmetric ring stretching vibrational mode lying at 968 cm^{-1} is now IR active, with a shift of −22.3 cm^{-1}. Although smaller than the 775 cm^{-1} band, relatively strong resonances are shown (see Figure 8c) by the in-plane C−H bend modes, centered at 992 and 1000 cm^{-1}, presenting reductions of −42 and −34.4 cm^{-1}, respectively. The in-plane carbon ring distortion modes were found at 1426 and 1431 cm^{-1} in the $Fe_6-C_6H_6$ complex, showing also noticeable reductions, −46.2 and −41.9 cm^{-1}, and a weak band. Thus, the calculated IR spectrum for this complex in the gas phase shows that, with respect to the bare benzene molecule, the out-of-plane C−H bend is shifted to the blue by 114 cm^{-1}, while the in-plane C−H bend and the in-plane carbon ring distortion are shifted to the red, by −42 to −34.4 cm^{-1} and −46.2 to −41.9 cm^{-1}, respectively. The frequency decrease of the last two bands is indicative of a weakened molecular bonding in the benzene moiety. Other non-IR active in-plane carbon ring distortions are more strongly diminished, by about −100 cm^{-1}, indicating a bigger decrease of the bonding in the benzene ring. For instance, the mode lying at 1588.2 cm^{-1} in free benzene is moved to 1488.2 cm^{-1} in the $Fe_6-C_6H_6$ complex. Indeed, the IR spectrum of $Fe_6-C_6H_6$ (see Figure 8c) shows that most of the frequencies of benzene are moved to lower values. One exception is the blue shift for the out-of-plane C−H bend, which is essentially a mechanical effect:[5] the presence of the Fe_6 cluster over the benzene ring impedes the out-of-plane hydrogen bend, driving the frequency higher. Even more, the C−H asymmetric stretching modes, at 3136 cm^{-1}, present also a small shift to the blue, of 14 cm^{-1}, that is mainly accounted for by the slight increase of the bonding in the C−H bonds; the C−H distances in free benzene, 1.089 Å, are slightly shortening to 1.087 Å, in $Fe_6-C_6H_6$. The full symmetric C−H stretching mode was located at the highest frequency, 3142 cm^{-1}, of the complex; it is IR inactive in free benzene but turns IR active in $Fe_6-C_6H_6$, with a small shift to the blue, 11 cm^{-1}, and a strong resonance. Hence, the C−H stretching modes suffer small shifts to the blue upon adsorption.

The bands within 67−400 cm^{-1} correspond either to Fe_6 or to induced Fe_6−benzene modes. For example, the strong (30.7 km/mol) resonance at 398 cm^{-1} is for an out-of-plane C−H bend, tied with oscillatory movements, along the axial direction, of the nearest Fe site. Similar details were found at 383 cm^{-1} but with 7.4 km/mol. The 336−345 cm^{-1} band is for swinging modes of benzene around the nearest Fe_a atom, with this one showing oscillations in a parallel direction to the benzene ring. At 327.4 cm^{-1}, the symmetric stretching of Fe_6 holds, showing a negligible intensity, 0.6 km/mol, and a shift of −9 cm^{-1}. The peaks at 262−281 cm^{-1} are for asymmetric stretching modes of Fe_6 in the equatorial plane, they are shifted to the blue by 17

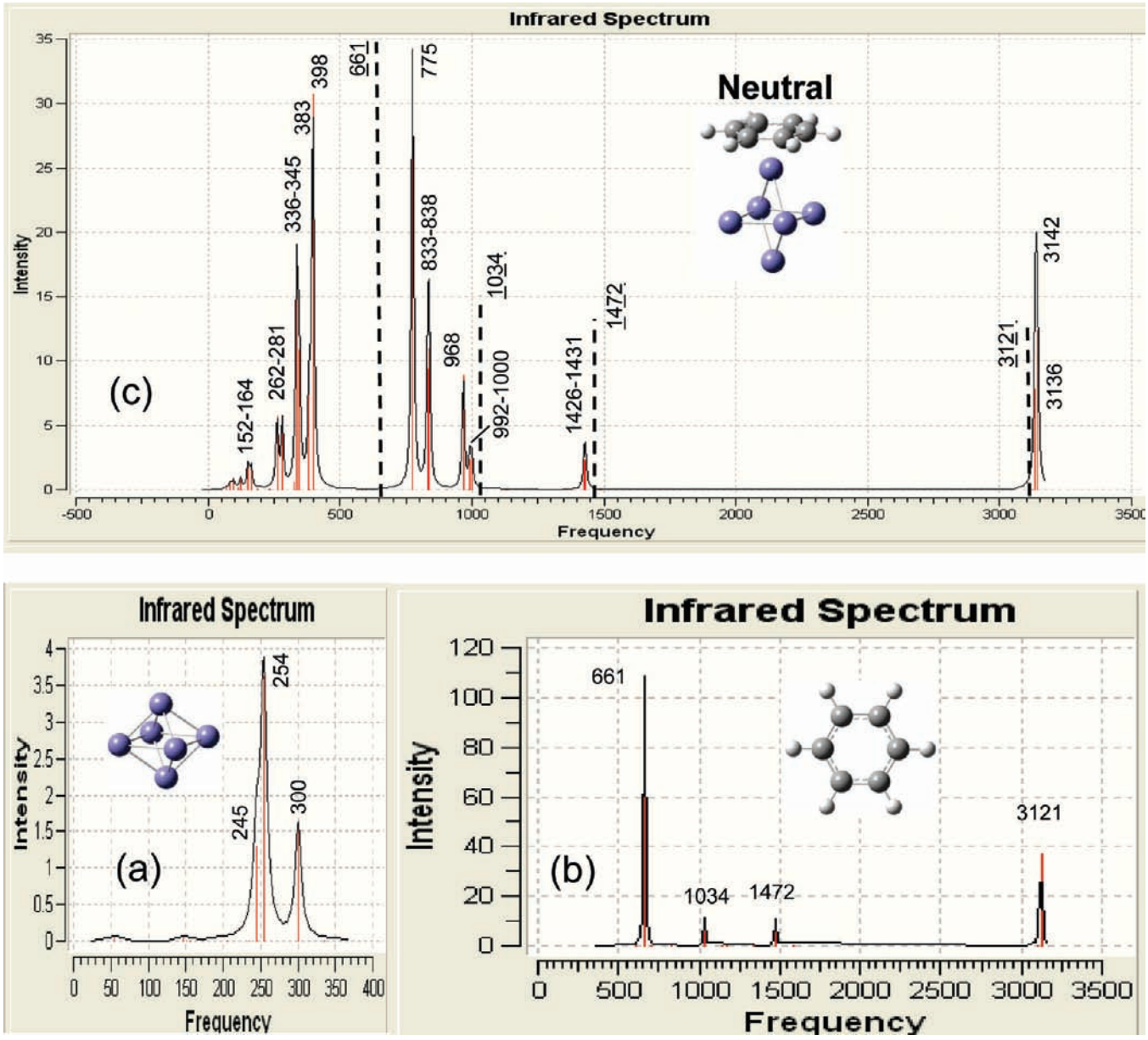

Figure 8. Calculated IR spectra for the neutral Fe_6 (c), C_6H_6 (a), and $Fe_6-C_6H_6$ (b) species.

and 27 cm^{-1}, with respect to bare Fe_6. As quoted above, the IR-active asymmetric stretching of free Fe_6 lies at 300 cm^{-1}; this mode lies at 232 cm^{-1} in the complex and is IR inactive. At 164 cm^{-1}, a symmetric stretching of Fe_6 holds, and at 152 cm^{-1} appears a swinging of benzene, with the nearest Fe site oscillating in a parallel direction of the benzene ring.

3f. Vibrational Analysis: Fe_6^+, $C_6H_6^+$, and $[Fe_6-C_6H_6]^+$. The calculated IR spectra of Fe_6^+, $C_6H_6^+$, and $[Fe_6-C_6H_6]^+$ are reported in Figure 9. The results, Figure 9b, show that $C_6H_6^+$ possess more IR-active bands than neutral benzene. The out-of-plane C−H bend, in-plane C−H bend, and in-plane carbon ring distortion modes, located at 657 (82), 1045 (10), and 1416−1502 cm^{-1} (105.2−46.3), are also IR active as in neutral benzene; from this reference, they are shifted by −4, 11, and −56 to +30 cm^{-1}. (Values in parentheses are for the intensities in km/mol.) The C−H asymmetric stretching modes, at 3144 and 3152 cm^{-1}, also remain IR active, and they are shifted to the blue by 23−31 cm^{-1}. Another IR-active C−H asymmetric stretching appears at 3125 cm^{-1}, with a minor intensity, and shows a shift of 29.5 cm^{-1}, with respect to neutral benzene, where it is IR inactive. These three CH frequencies originate the upper band for the IR spectrum of the $C_6H_6^+$ ion. The band at 1377 cm^{-1} is for an in-plane carbon ring distortion, shifted to the blue by 47 cm^{-1}, with respect to the IR-inactive mode in C_6H_6. An in-plane C−H bend mode positioned at 942 cm^{-1} shows a modest intensity and also contributes to the IR spectrum; weaker bands appear at 971 and 268 cm^{-1}, which are for out-of-plane C−H bends. Contrary to C_6H_6 and $C_6H_6^+$, the IR spectrum for the Fe_6^+ ion is not quite different from that of the neutral Fe_6 cluster. Indeed, as shown in Figures 8a and 9a, the Fe_6^+ ion also presents three main IR-active bands, having higher intensities and shifted to lower frequencies, which are for the vibrational modes described above for Fe_6.

The IR spectrum for the $[Fe_6-C_6H_6]^+$ cation is shown in Figure 9c, and in Table 5 are reported the vibrational frequencies that the benzene molecule presents in this complex. Since the IE of Fe_6, 6.15 eV, is considerably smaller than that of benzene, 9.08 eV, it is expected that electron detachment from $Fe_6-C_6H_6$ mainly occurs from the Fe_6 fragment, producing an $[Fe_6-C_6H_6]^+$ ion that could be viewed as an Fe_6^+ moiety joined to benzene. Indeed, the IR spectrum of $[Fe_6-C_6H_6]^+$ reveals the presence of vibrational bands, which are nearer to those of neutral benzene

TABLE 4: Estimated Vibrational Frequencies and Intensities for Bare Benzene[a]

		benzene			benzene in $Fe_6-C_6H_6$			
		theory						
	mode	ν (cm^{-1})	I (km/mol)	exp.[c] ν (cm^{-1})	error (%)	ν (cm^{-1})	I (km/mol)	$\Delta\nu$ (cm^{-1})
1	γ(CCC)	394[b]		410	3.9	383.1	7.4	−10.9
2	γ(CCC)	394		410	3.9	384.5		−9.5
3	δ(CCC)	603.1		606	0.48	598.7		−4.4
4	δ(CCC)	603.2		606	0.49	597.8		−5.4
5	γ(C−H)	661.1	108.7	673	1.77	775.1	34.3	114
6	γ(CCC)	699		703	0.57	586.3		−112.7
7	γ(C−H)	830.6[b]		849	2.17	833.4	9.4	2.8
8	γ(C−H)	830.7[b]		849	2.17	837.6	10.9	6.9
9	γ(C−H)	946.8		975	2.89	875.4		−71.4
10	γ(C−H)	946.8		975	2.89	876.2		−70.7
11	γ(C−H)	976.4		995	1.9	904		−72.4
12	δ(CCC)	989.9[b]		992	2.02	967.5	8.9	−22.3
13	δ(C−C)	997.6		1010	1.23	988.7		−8.9
14	δ(C−H)	1034.2	5.8	1038	3.85	992.1	2.4	−42
15	δ(C−H)	1034.2	5.8	1038	3.85	999.8	2.5	−34.4
16	δ(C−H)	1146.7		1150	2.61	1137.1		−9.6
17	δ(C−H)	1167.3		1178	0.94	1129.3		−38
18	δ(C−H)	1167.3		1178	0.94	1131.4		−35.9
19	ν(C═C)	1330.7		1310	1.58	1389.4		−58.8
20	δ(C−H)	1342.9		1326	1.27	1317.7		−25.3
21	δ(CCC)	1472.4	6.1	1486	0.92	1426.2	2.3	−46.2
22	δ(CCC)	1472.4	6.1	1486	0.92	1430.5	2.3	−41.9
23	ν(C═C)	1588.2		1596	0.49	1488.2		−100
24	ν(C═C)	1588.2		1596	0.49	1484.2		−104
25	δ(C−H)	3095.9		3047	1.60	3119.6		23.7
26	ν'(C−H)	3105.5		3062	1.42	3125.2		19.7
27	ν'(C−H)	3105.6		3062	1.42	3125.8		20.2
28	ν'(C−H)	3121.1	36.8	3063	1.89	3135.7	7.9	14.6
29	ν'(C−H)	3121.1	36.8	3063	1.89	3135.8	7.6	14.7
30	δ(C−H)	3131.5[b]		3068	2.07	3142.2	12.4	10.7

[a] The values that benzene presents in the $Fe_6-C_6H_6$ complex are shown. The experimental values for benzene and the errors of the calculations are also indicated. The nomenclature is as follows: "out of plane bending" (γ), "in plane bending" (δ), "symmetric stretching" (ν), and "asymmetric stretching" (ν'). [b] IR active in the neutral $Fe_6-C_6H_6$ complex. [c] Experimental values from ref 46.

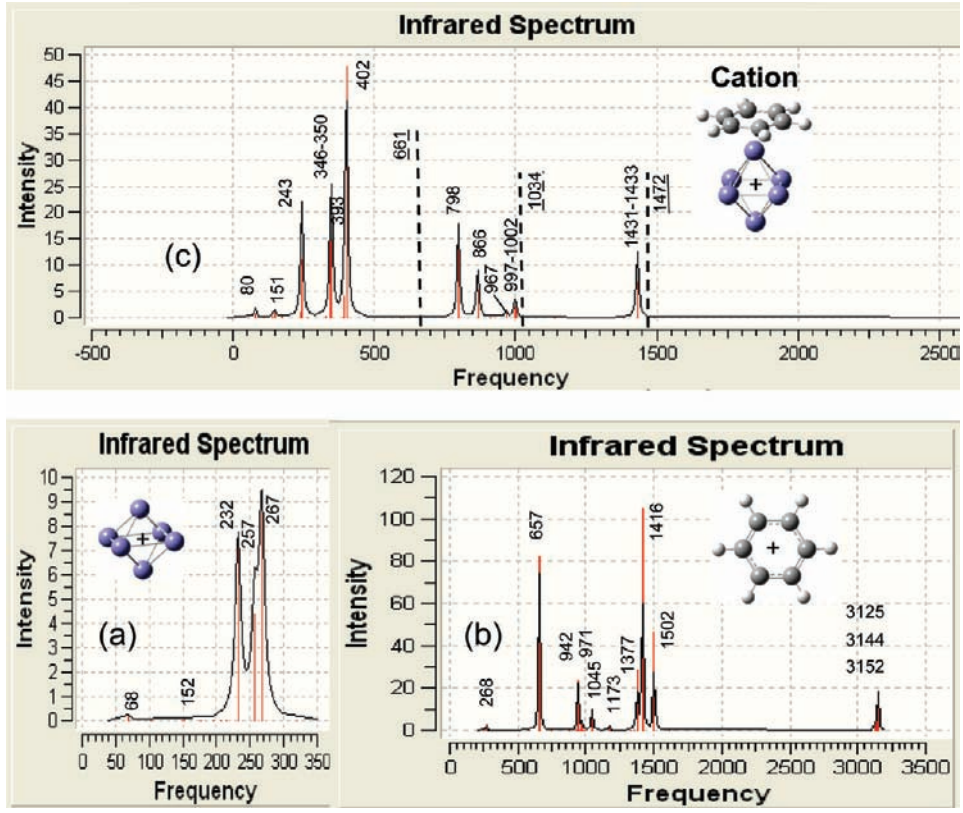

Figure 9. Calculated IR spectra for the Fe_6^+ (c), $C_6H_6^+$ (a), and $[Fe_6-C_6H_6]^+$ (b) cations.

than to those of $C_6H_6^+$; see Table 5. The dashed lines in Figure 9c are for IR-active modes of neutral benzene. The results also indicate that some IR-inactive modes of free benzene become IR active in the reduced symmetry of the complex. Conversely,

TABLE 5: Calculated Frequencies and Intensities for the Bare Benzene$^+$ Ion[a]

		bare benzene$^+$		benzene in $[Fe_6-C_6H_6]^+$			
	mode	ν (cm^{-1})	I (km/mol)	ν (cm^{-1})	I (km/mol)	$\Delta\nu$ (cm^{-1})[d]	$\Delta\nu$ (cm^{-1})[e]
1	δ(CCC)	240.3		595.3		355	−7.8
2	γ(CCC)	268	2.6	392.8	4	124.8	−1.1
3	γ(CCC)	322.3		391		68.7	−2.9
4	γ(C−H)	324.6		605.1		280.6	−93.9
5	δ(CCC)	584.8		596.1		11.3	−7.0
6	γ(C−H)	657.1	82.1	797.9	17.9	140.9	+136.8
7	γ(C−H)	754.3[b]		866.2	5.3	112	+35.5
8	γ(C−H)	875.4[b]		867.2	4.7	−8.3	+86.5
9	δ(C−H)	925.2		996.9	2	71.7	−34.3
10	δ(C−H)	941.7	23.4	1001.5	1.7	59.9	−32.7
11	δ(CCC)	955.5[b]		967.1	1.3	11.6	−22.8
12	γ(C−H)	971.1[c]	4.3	911.9		−59.2	−34.9
13	γ(C−H)	982.8		909.8		−73	−37.0
14	δ(CCC)	985.6	0.1	998.9	0.5	13.3	+1.3
15	γ(C−H)	1000.8		929.6		−71.2	−46.8
16	δ(C−H)	1045	10.1	1136.6		91.6	30.7
17	δ(C−H)	1173.3[c]	2	1144.3		−29	−2.4
18	δ(C−H)	1187.5		1137.6		−49.9	−29.7
19	δ(C−H)	1333.8		1493.4		159.6	−94.8
20	δ(C−H)	1351.8		1322.6		−29.2	−20.4
21	δ(CCC)	1377.4	28.8	1382.5	0.2	5.2	+51.9
22	δ(CCC)	1416.3	105.2	1433.2	6.8	17	−39.2
23	δ(CCC)	1502.4	46.3	1431	6.5	−71.4	−41.4
24	ν(C═C)	1619.8[b]		1491.3	0.1	128.5	−96.9
25	ν'(C−H)	3125.4[c]	1.8	3130.7		5.3	+34.8
26	ν(C−H)	3129.1		3134.5		5.3	+29.0
27	ν(C−H)	3141		3137.0		−39.6	+31.4
28	ν'(C−H)	3144[c]	8.7	3144.8		−0.8	+23.7
29	ν'(C−H)	3152.4[c]	16.4	3146.7		−5.7	+25.6
30	ν(C−H)	3155.3[b]		3151.8	0.2	−3.5	+20.3

[a] The values that benzene presents in the $[Fe_6-C_6H_6]^+$ complex are shown. The nomenclature is the same as in Table 4. [b] IR active in the $Fe_6-C_6H_6^+$ complex. [c] IR inactive in the $Fe_6-C_6H_6^+$ cation. [d] With respect to the benzene$^+$ cation. [e] With respect to neutral benzene.

some high frequency IR-active modes of bare benzene become IR inactive. We proceed with the description of these features. At 798 cm^{-1}, the band for the out-of-plane C−H bending is located with a smaller intensity (18 km/mol) but shifted to the blue, by 137 cm^{-1} with respect to C_6H_6, more strongly than in the neutral $Fe_6-C_6H_6$ complex (114 cm^{-1}), which is a signature of a stronger mechanical effect in $[Fe_6-C_6H_6]^+$: the presence of the Fe_6^+ cluster over the benzene ring increases the impediment for the out-of-plane hydrogen bending, because an additional electrostatic repulsion between Fe_6^+ and the $H^{\delta+}$ atoms now appears, i.e., the C−H bond has some polar behavior. In fact, of the studied neutral and charged species, this mode in this complex presents the largest shift to the blue. At 997−1002 cm^{-1}, the in-plane C−H bends were found with minor intensities but with similar shifts to the red, −32.7 to −34.3 cm^{-1}, as those of neutral $Fe_6-C_6H_6$, −34.4 to −42 cm^{-1}. The weak band at 967 cm^{-1} is for the symmetric ring stretching, which is IR inactive in $C_6H_6^+$, at 956 cm^{-1}, and in neutral C_6H_6, at 990 cm^{-1}. At 866.2 cm^{-1}, a modest resonance for an out-of-plane C−H bending of four CH units is located; this mode is IR inactive in neutral benzene, at 830.7 cm^{-1}, and in $C_6H_6^+$, at 754.3 cm^{-1}. So, this mode is shifted to the blue by 35.5 cm^{-1} and by 112 cm^{-1}. See Table 5. The upper band, 1431−1433 cm^{-1}, is for two in-plane carbon ring distortions with modest intensities, 6.8 km/mol, and is shifted to the red by $\cong$−40 cm^{-1}, with respect to the neutral benzene molecule.

Up to here, these results indicate that the out-of-plane C−H bend, the in-plane C−H bend, and the in-plane carbon ring distortion modes of benzene, in the $[Fe_6-C_6H_6]^+$ complex, are shifted by +137, −32.7 to −34.3, and −40 cm^{-1}, respectively. The displacement to the red for the last two bands is indicative of a weakening of the molecular bonding in the benzene moiety. On the other hand, the observed IR spectrum for positively charged TM atoms binding to benzene in the condensed phase also shows similar vibrational shifts; that is, with respect to the neutral benzene molecule, the out-of-plane C−H bend occurs at higher frequencies while the in-plane C−H bend and the in-plane carbon ring distortion are moved to the red.[5] Lastly, the IR spectrum for C_6H_6 and $C_6H_6^+$ shows that the asymmetric C−H stretching modes, lying at highest frequencies, are IR active; see Figures 8b and 9b. However, these modes becomes IR inactive in the $[Fe_6-C_6H_6]^+$ cation.

At a low frequency, 402 cm^{-1}, the strongest band of this complex is located, which exhibits similar features as the mode lying at 398 cm^{-1} of the neutral $Fe_6-C_6H_6$ complex. With a smaller intensity, an analogous behavior was found for the mode lying at 393 cm^{-1}. The notorious band at 346−350 cm^{-1} mimics the vibrational modes of $Fe_6-C_6H_6$ lying at 336−345 cm^{-1}. The modest band positioned at 243 cm^{-1} accounts for two asymmetric stretching modes between two equatorial Fe atoms of the cluster, coupled with swinging movements of benzene. The small band at 151.2 cm^{-1} (1.4 km/mol) accounts for the symmetric stretching of the Fe_6^+ fragment. Finally, the bands at 78−79.5 cm^{-1} are swinging modes of benzene around the Fe_6^+ cluster.

3g. Vibrational Analysis: Fe_6^-, $C_6H_6^-$, and $[Fe_6-C_6H_6]^-$. The IR spectrum of the $C_6H_6^-$ ion, Figure 10b, is similar to that of neutral benzene. Effectively, with enhanced resonances, only the out-of-plane C−H bend (676.4 cm^{-1}), the in-plane C−H bend (1029 cm^{-1}), the in-plane carbon ring distortion (1469 cm^{-1}), and the asymmetric C−H stretching (3056.2 cm^{-1}) modes are IR active. With respect to the neutral, the first mode shows a small shift to the blue, of 15 cm^{-1}, the second and third shifts have minor reductions, −5 and −3 cm^{-1}, and the last one is more clearly moved, by −65 cm^{-1}, to the red. So, one electron addition produces relatively small changes on the IR spectrum of benzene, mainly accounted for by the fact that the electron goes into a higher energy nonbonding orbital. As

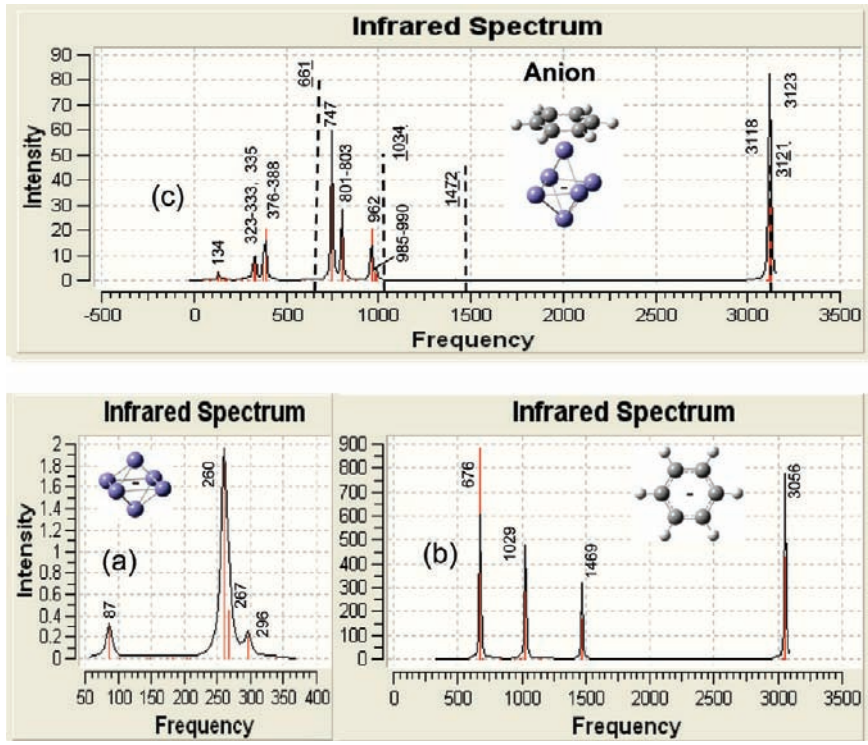

Figure 10. Calculated IR spectra for the Fe_6^- (c), $Fe_6-C_6H_6^-$ (a), and $[Fe_6-C_6H_6]^-$ (b) anions.

in the neutral Fe_6 cluster, the IR spectrum for the Fe_6^- anion, Figure 10a, also possesses three IR-active modes lying at 296, 267, and 260 cm^{-1}, with noticeably smaller intensities; the first two are shifted to the blue by 23 and 6 cm^{-1}, and the last one is shifted by -4 cm^{-1}. Also, with a small intensity, a peak appears at 87 cm^{-1}, being shifted to the blue by 32 cm^{-1}. The symmetric stretching of Fe_6^-, 338 cm^{-1}, is IR inactive with a minor shift of 2 cm^{-1}. Thus, most of the IR bands of Fe_6^- are slightly shifted to higher values, which reflects the fact that it is more stable, by 1.61 eV, than the neutral, with an increase in the bonding, since the average bond length of the Fe_6^- anion, 2.389 Å, is shorter than that of Fe_6, 2.404 Å.

The IR spectrum for the $[Fe_6-C_6H_6]^-$ anion is shown in Figure 10c, and in Table 6 are indicated the frequencies that the benzene moiety presents in this complex. The added electron to $Fe_6-C_6H_6$, $M = 17$, goes into its LUMO$^\downarrow$ orbital (shown in Figure 5 of the Supporting Information) to yield the $M = 16$ state for $[Fe_6-C_6H_6]^-$; since the LUMO has a major contribution on Fe_6, such an electron mainly resides on the metallic part of the complex. Then, it will be more appropriate to evaluate the shifts of benzene, in $[Fe_6-C_6H_6]^-$, with respect to neutral bare benzene, instead of choosing the $C_6H_6^-$ anion. However, similar results are obtained for both references. See Table 6. For example, the IR-active out-of-plane C−H bend, at 747 cm^{-1}, showing also a strongest band (as in $Fe_6-C_6H_6$, C_6H_6, and $C_6H_6^-$) is shifted to the blue by 71 or by 86 cm^{-1}. Two other out-of-plane C−H bend modes, at 801 and 803 cm^{-1}, were found also to be IR active with moderate intensities and shifted to the red by $\cong -30$ cm^{-1}; see Table 6 and Figure 10c. As quoted, the IR-active in-plane C−H bend lies at a similar frequency, 1034 and 1029 cm^{-1}, in free neutral and negative benzene; in $[Fe_6-C_6H_6]^-$, this mode was found at the 985−990 cm^{-1} weak band and is clearly shifted to the red, with respect to both C_6H_6 and $C_6H_6^-$. Likewise, the in-plane carbon ring distortion (IR active in bare neutral and anionic benzene species) was found at 1419 and 1422 cm^{-1} in $[Fe_6-C_6H_6]^-$ and is essentially IR inactive, because these frequencies have minor intensities; see Table 6. Either from bare C_6H_6 or $C_6H_6^-$, this mode is shifted to the red, by $\cong -50$ cm^{-1}. The shift to the red for the in-plane C−H bend and the in-plane carbon ring distortion, by -44 to -49 cm^{-1} and by -50 cm^{-1}, respectively, also implies a weakening of the molecular bonding for benzene in the $[Fe_6-C_6H_6]^-$ complex. Note that these shifts are slightly bigger than those of $Fe_6-C_6H_6$ and $[Fe_6-C_6H_6]^+$; thus, in $[Fe_6-C_6H_6]^-$, a (slightly) bigger reduction for the molecular bonding of benzene occurs. The experimental determination of these frequency displacements will be valuable to confirm or deny this tendency. Moreover, the symmetric ring stretching, IR inactive in bare benzene and $C_6H_6^-$ and lying at 990 cm^{-1} in both cases, becomes IR active in $[Fe_6-C_6H_6]^-$, at 962 cm^{-1}, with a notorious band and becomes shifted to the red by a slightly bigger value, -28 cm^{-1}, than in the other complexes. We now move to the highest frequencies; the asymmetric C−H stretching band, at 3118 cm^{-1}, remains IR active with a negligible decrease, of -3.4 cm^{-1}, with respect to the free benzene molecule but clearly is shifted to the blue, by 61.5 cm^{-1}, with respect to the bare $C_6H_6^-$ anion. A similar picture holds for the symmetric C−H stretching, which is IR inactive in bare C_6H_6 and $C_6H_6^-$ but turns IR active in the complex at 3123.8 cm^{-1}, which shows the strongest band. At low frequencies, the modes lying at 376−388, 335, and 323−333 cm^{-1} mimic the 383−398, 327, and 336−345 cm^{-1} modes, respectively, of neutral $Fe_6-C_6H_6$ described above. At 260 cm^{-1} with 1.8 km/mol, an asymmetric stretching of bare Fe_6^- was found; in neutral Fe_6, this mode lies at 254 cm^{-1} with 3.6 km/mol, and this mode is located at 293 cm^{-1} in $Fe_6-C_6H_6^-$, where it is IR inactive. Lastly, at the bottom of the IR spectrum of $[Fe_6-C_6H_6]^-$ lies the 134 cm^{-1} (3.4 km/mol) band, which is for the symmetric stretching of the Fe_6 moiety; this mode is IR inactive in neutral Fe_6, lying at 116 cm^{-1}, and in the Fe_6^- anion, at 147 cm^{-1}.

3h. Vibrational Analysis: $Fe_6-(C_6H_6)_2$, $[Fe_6-(C_6H_6)_2]^+$, and $[Fe_6-(C_6H_6)_2]^-$. The IR spectrum of $Fe_6-(C_6H_6)_2$ is shown in Figure 11a. In this case, the out-of-plane C−H bend also presents a very strong resonance at 752 cm^{-1} but is shifted to

TABLE 6: Calculated Frequencies and Intensities for the Bare Benzene$^-$ Ion[a]

	bare benzene$^-$ anion			benzene in $[Fe_6-C_6H_6]^-$			
	mode	ν (cm^{-1})	I (km/mol)	ν (cm^{-1})	I (km/mol)	$\Delta\nu$ (cm^{-1})[d]	$\Delta\nu$ (cm^{-1})[e]
1	γ(CCC)	364.5		377.8		13.3	−16.1
2	γ(CCC)	364.6[b]		387.7	20.6	23.1	−6.2
3	δ(CCC)	593.3		597.8		4.5	−5.4
4	δ(CCC)	593.7		597.8		4.1	−5.3
5	γ(C−H)	676.4	879.0	747.4	59.7	71.0	86.3
6	γ(CCC)	690.3		557.2		−133.1	−141.8
7	γ(C−H)	833.5[b]		802.6	15.0	−31.0	−28.1
8	γ(C−H)	834.2[b]		801.2	16.4	−32.9	−29.4
9	γ(C−H)	946.0		836.1		−109.9	−110.7
10	γ(C−H)	946.2		837.3		−108.9	−109.5
11	γ(C−H)	982.1		872.5		−109.6	−103.9
12	δ(CCC)	988.3		978.4		−9.9	−19.2
13	δ(CCC)	990.0[b]		962.0	20.8	−28.0	−27.9
14	δ(C−H)	1029.1	391.0	985.3	2.8	−43.8	−48.9
15	δ(C−H)	1029.2	385.0	989.9	2.8	−39.2	−44.3
16	δ(C−H)	1132.1	0.1	1128.5	0.1	−3.6	−18.2
17	δ(C−H)	1145.6		1121.6	0.1	−23.9	−45.7
18	δ(C−H)	1145.6		1119.2		−26.4	−48.1
19	δ(CCC)	1336.7		1386.5		49.8	55.8
20	δ(C−H)	1339.7		1311.2		−28.4	−31.7
21	δ(CCC)	1469.3[c]	166.5	1419.4	0.2	−50.0	−53.2
22	δ(CCC)	1469.4[c]	165.4	1422.0	0.3	−47.5	−50.5
23	ν'(C=C)	1579.5		1474.9		−104.6	−113.2
24	ν'(C=C)	1579.6		1473.6		−106.0	−114.7
25	ν' (C−H)	3034.2		3100.6		66.4	4.7
26	ν(C−H)	3046.3[b]		3123.8	52.5	77.5	−7.7
27	ν'(C−H)	3053.8		3106.4		52.6	0.9
28	ν'(C−H)	3053.9		3107.8		53.9	2.2
29	ν'(C−H)	3056.2	415.5	3117.7	31.3	61.5	−3.4
30	ν'(C−H)	3056.2	430.9	3117.0	30.1	60.8	−4.0

[a] The values that benzene presents in the $[Fe_6-C_6H_6]^-$ complex are shown. The nomenclature is the same as in Table 4. [b] IR active in the $Fe_6-C_6H_6^+$ complex. [c] IR inactive in the $Fe_6-C_6H_6^+$ ion. [d] With respect to the $C_6H_6^+$ ion. [e] With respect to neutral benzene.

the blue by a smaller amount, 91 cm^{-1}, than in $Fe_6-C_6H_6$, 114 cm^{-1}, suggesting a smaller impediment of Fe_6 for this type of bending. The modest band at 822−823 cm^{-1} is for out-of-plane C−H bend modes, showing small shifts, −9 to −8 cm^{-1}. Weak bands appear for the in-plane C−H bend, at 990−991 cm^{-1}, and for the in-plane carbon ring distortion, at 1424−1426 cm^{-1}, which present shifts similar to the red, −43 and −46 cm^{-1}, as those found for $Fe_6-C_6H_6$, indicating also a weakening of the bonding for the benzene molecules in $Fe_6-(C_6H_6)_2$. Besides, the symmetric ring stretching of each benzene, lying at 947 cm^{-1} with a prominent band (35 km/mol), is shifted to the red more strongly, by −53 cm^{-1}, than in the neutral and charged monobenzene complexes, $[Fe_6-C_6H_6]^{\pm}$, where it is shifted by −22 to −28 cm^{-1}. Here, the stretching of one benzene molecule is out of phase from the other one. When the symmetric ring stretching modes of the two benzene units are in phase, the whole mode is IR inactive and lies at a higher frequency, 961 cm^{-1}, with a smaller displacement, −29 cm^{-1}. With a modest intensity, 23 km/mol, an asymmetric C−H stretching is located at 3134 cm^{-1}. The symmetric C−H stretching modes of the two benzene units, in the out-of-phase way, lie at 3140 cm^{-1} and show a strongest resonance, 44 km/mol. The in-phase symmetric C−H stretching mode is non-IR active and is situated quite close, at 3141 cm^{-1}. We now address the low-frequency part; the weak band at 583 cm^{-1} is for in-plane carbon ring distortions. The resonance at 375 cm^{-1} is mainly for out-of-plane C−H bend modes of the two benzenes coupled with oscillatory movements of the two axial Fe_a atoms along the axial direction. The 313−318 cm^{-1} band is for swinging movements of the benzene units tied with bending modes of the axial Fe sites. At 289 cm^{-1}, the strongest band of $Fe_6-(C_6H_6)_2$ lies here; the two axial Fe_a atoms oscillate rigidly (their internuclear length does not change) along the axial direction and are coupled with out-of-plane C−H bend modes of the benzene moieties. The 285−259 cm^{-1} band, 4.5−1 km/mol, is for in-plane distortions of the iron equatorial sites tied with swinging modes of benzene. The small band at 178 cm^{-1}, 1.4 km/mol, shows swinging movements of benzene tied with bend modes of the two axial Fe atoms. Similar features are observed at 132 cm^{-1}. Lastly, the weak band at 89 cm^{-1}, with 4.9 km/mol, is for a stretching of the whole Fe_6 cluster with the two benzene moieties.

The estimated IR spectrum for $[Fe_6-(C_6H_6)_2]^+$ is shown in Figure 11b. Here, the out-of-plane C−H bend, 772 cm^{-1}, shows a bigger shift to the blue, 111 cm^{-1}, than that of neutral $Fe_6-(C_6H_6)_2$, 91 cm^{-1}. This tendency is similar to that observed for $[Fe_6-C_6H_6]^+$ and $Fe_6-C_6H_6$, which present shifts to the blue of 137 and 114 cm^{-1}, respectively. Note that these last two complexes are the ones that present the biggest displacement to the blue for this mode. The in-plane C−H bending lies at 996 cm^{-1}; this weak band is shifted to the red by about the same amount, −38 cm^{-1}, as in $[Fe_6-C_6H_6]^+$, −34.3 to −32.7 cm^{-1}. The magnitude of these shifts are slightly smaller than those of the neutral $Fe_6-(C_6H_6)_{1,2}$ complexes, quoted above. Also the in-plane carbon ring distortion of $[Fe_6-(C_6H_6)_2]^+$ falls at about the same value, 1431 cm^{-1}, as that of $[Fe_6-C_6H_6)]^+$, 1431−1433 cm^{-1}, producing a shift to the red of −42 cm^{-1}. Thus, these results show that the frequency shifts in $[Fe_6-(C_6H_6)_2]^+$ are equal to +111, −38, and −42 cm^{-1}, for the out-of-plane C−H bend, in-plane C−H bend, and in-plane carbon ring distortion, respectively. The shifts to the red for the last two modes are indicative of a decrease of the molecular bonding for the benzene moieties in the $[Fe_6-(C_6H_6)_2]^+$ complex. Further, in the out-of-phase way, the symmetric ring stretching of the two benzene moieties was located at 953 cm^{-1}, and showing a weak band, it was also shifted to the red, by −47 cm^{-1}. The in-phase symmetric ring stretching of the benzene moieties is IR inactive and lies at 962 cm^{-1}. Note that these last frequencies are close to those of the $Fe_6-(C_6H_6)_2$

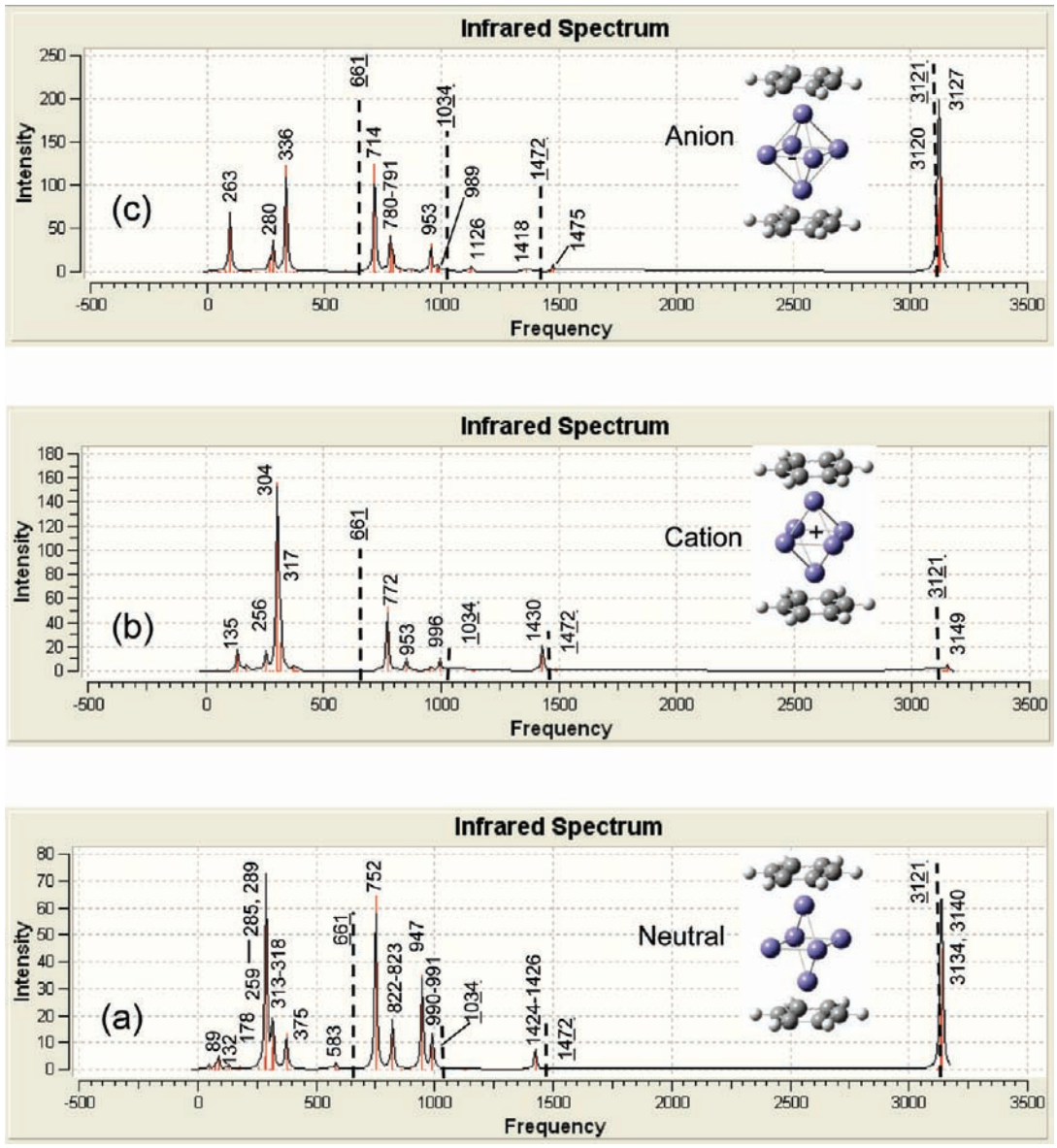

Figure 11. Calculated IR spectra for $[Fe_6-(C_6H_6)_2]$ (a), $[Fe_6-(C_6H_6)_2]^+$ (b), and $[Fe_6-(C_6H_6)_2]^-$ (c).

adduct, 947 and 961 cm^{-1}. On the other hand, for the dibenzene $Fe^+(C_6H_6)_2$ complex the displacements for the out-of-plane C−H bend, in-plane C−H bend, and in-plane carbon ring distortion have been determined by means of the FELIX free electron laser technique. As shown in Figure 12 of ref 5, the measured values, of about +93, −67, and −40 cm^{-1}, follow a tendency similar to those obtained for $Fe_6^+-(C_6H_6)_2$ in the present work: +111, −38, and −42 cm^{-1}, which shows encouragement since it means that the shifts of the $Fe_6-(C_6H_6)_{1,2}$ ions could be determined by the FELIX method or probably also by the use of infrared multiple-photon dissociation (IRMPD) spectroscopy, applied successfully to the study of Fe−PAH ions.[11]

The small peak in the IR spectrum of $[Fe_6-(C_6H_6)_2]^+$ lying at 3149 cm^{-1} corresponds to the symmetric C−H stretching of the benzene molecules, in the out-of-phase way; note the absence of this feature in the IR spectrum of $[Fe_6-C_6H_6]^+$. The in-phase symmetric C−H stretching is IR inactive and lies at the top frequency, 3150 cm^{-1}, of the complex. At low frequencies, the band at 317 cm^{-1} is for swinging modes of the benzene molecules coupled with oscillatory movements, in a parallel direction to the benzene rings, of the two axial iron atoms. At 304 cm^{-1}, the strongest band is positioned, which is quite similar to the vibrational mode of $Fe_6-(C_6H_6)_2$ at 289 cm^{-1}. The small band at 256 cm^{-1} mimics the mode of $Fe_6-(C_6H_6)_2$ lying at 285 cm^{-1}. Lastly, the small peak at 135 cm^{-1} is for a stretching mode of the whole Fe_6 cluster with the two benzene molecules.

Of the studied species, $[Fe_6-(C_6H_6)_2]^-$ shows the smallest shift to the blue, 53 cm^{-1}, for the out-of-plane C−H bend, lying at 714 cm^{-1} with the strongest resonance (see Figure 11c), implying the smallest impediment for this type of vibrational mode, which is partially accounted for by the fact that in this complex occurs the longest Fe−C distances, 2.14−2.17 Å, as compared for example with those of $Fe_6-(C_6H_6)_2$, which are limited within 2.13−2.14 Å. The modest band lying at 780−791 cm^{-1} also corresponds to out-of-plane C−H bend modes, but they involve the bending of only four or three CH units. The in-plane C−H bend is located at 989 cm^{-1} with a negligible band, 1 km/mol, and shifted to the red by −45 cm^{-1}. Unexpectedly, another in-plane C−H bend lies at 1126 cm^{-1} with a higher intensity, 6.3 km/mol, but shifted to the blue by 92 cm^{-1}. Also, with a negligible band, 1.6 km/mol, the in-plane carbon ring distortion is located at 1418 cm^{-1}, yielding a negative shift of −54 cm^{-1}. Another in-plane carbon ring distortion lies at about the same frequency, 1475 cm^{-1}, as that of bare benzene, 1472

cm^{-1}; its intensity, 8.7 km/mol, is also quite similar (see Table 4). Then, showing very weak resonances, the in-plane C−H bend and the in-plane carbon ring distortion modes are shifted to the red by −45 and −54 cm^{-1}, respectively, suggesting also a weakening of the molecular bonding of the benzene ligands in the $[Fe_6-(C_6H_6)_2]^-$ complex.

As shown above, the in-plane carbon ring distortion is IR inactive in $[Fe_6-C_6H_6]^-$ and, in $[Fe_6-(C_6H_6)_2]^-$, though the band is quite weak, the IR activity of this mode is recovered. Furthermore, the symmetric ring stretching mode of the two benzene molecules, in the out-of-phase way, is situated at the same frequency, 953 cm^{-1}, and shows also the same shift to the red, −47 cm^{-1}, as in $[Fe_6-(C_6H_6)_2]^+$, but with an enhanced resonance; see Figure 11c. Similarly, the in-phase symmetric ring stretching of the rings, at 956 cm^{-1}, is IR inactive. Centered at 3120 cm^{-1} is located a strong band for three asymmetric C−H stretching modes. Closely, at 3127 cm^{-1}, lies the strongest resonance of $[Fe_6-(C_6H_6)_2]^-$, which is for the (out-of-phase) symmetric C−H stretching modes of the benzene moieties; these last two frequencies show minor shifts to the red, −1 and −5 cm^{-1}, respectively, with respect to neutral benzene. At low frequencies, 336 cm^{-1}, the strongest band for the IR spectrum of $[Fe_6-(C_6H_6)_2]^-$ also appears, which is for a similar mode as that located at 304 cm^{-1} for $[Fe_6-(C_6H_6)_2]^+$ and at 289 cm^{-1} for $Fe_6-(C_6H_6)_2$, which also show the strongest resonances. With a modest intensity, the band situated at 280 cm^{-1} mimics the vibrational mode lying at 256 cm^{-1} for $[Fe_6-(C_6H_6)_2]^+$ and at 285 cm^{-1} for $Fe_6-(C_6H_6)_2$. At the bottom of the spectrum, 263 cm^{-1}, lies a modest band, which accounts for swinging modes of benzene coupled with oscillatory movements, in a parallel direction to the benzene rings, of a square defined by two axial and two equatorial iron atoms.

4. Conclusions

The interactions of one and two benzene molecules with the magnetic Fe_6 cluster were studied with the BPW91/6311++G(2d,2p) method. The theoretical results for the IE and EA of Fe_6 are in close agreement with the experimental values, which gives support in that the $M = 21$ distorted octahedral structure is the GS of this cluster, and that the chosen method describes properly the metal−metal interactions in this kind of magnetic particles. Other spin states of Fe_6 produce EAs and IEs that differs significantly from the experimental results. It was found that the adsorption of benzene considerably reduces the magnetic moment of Fe_6. The total magnetic moments for the GS of $Fe_6-C_6H_6$, 16 μ_B, and $Fe_6-(C_6H_6)_2$, 14 μ_B, are quenched by about 4 and 6 μ_B, respectively, as compared with the bare Fe_6 cluster, 20 μ_B. Also, adsorption of two benzenes produces a shrinking of Fe_6, indicating an increase of the metal−metal bonding. Thus, magnetic effects are crucial in the adsorption of C_6H_6 by Fe_6. The estimated adiabatic BDEs per benzene: 20−24 kcal/mol for $Fe_6-(C_6H_6)_{1,2}$, ≅38 kcal/mol for $[Fe_6-(C_6H_6)_{1,2}]^+$, and 16−17 kcal/mol for $[Fe_6-(C_6H_6)_{1,2}]^-$, give insight that the $Fe_n(C_6H_6)_m$ structures, as proposed experimentally, consist of an Fe_n core surrounded by adsorbed benzene molecules.[7] The BDEs are accounted for by electrostatic and by 3d−π covalent contributions. Though each C−Fe bond is weak, 3−6 kcal/mol, η^6 coordinations on these compounds were confirmed by the topological properties of the electronic density. Consistently, the decrease of the IEs is a clear signature of d−π interactions; the EAs are also diminished. The calculated IR spectra for the complexes present vibrational bands near those of the free benzene molecule, and some forbidden IR modes in benzene become IR active in the complexes. Conversely, some IR-active modes in benzene become inactive in the $[Fe_6-(C_6H_6)_{1,2}]^{+,-}$ charged complexes.

The out-of-plane C−H bend modes are displaced to the blue by 91−114 cm^{-1} for $Fe_6-(C_6H_6)_{1,2}$, 111−137 cm^{-1} for $Fe_6-(C_6H_6)_{1,2}]^+$, and 53−86 cm^{-1} for $[Fe_6-(C_6H_6)_{1,2}]^-$; in each case, the smaller value is for $m = 2$. Thus, the cations (anions) show the biggest (smallest) impediment for this type of C−H bending. The in-plane C−H bend modes are shifted to the red by similar quantities in these compounds: −34 to −43 cm^{-1} for $Fe_6-(C_6H_6)_{1,2}$, −32 to −38 cm^{-1} for $[Fe_6-(C_6H_6)_{1,2}]^+$, and −44 to −49 cm^{-1} for $[Fe_6-(C_6H_6)_{1,2}]^-$. Analogously, the in-plane carbon ring distortions are shifted to the red by −42 to −47 cm^{-1} for $Fe_6-(C_6H_6)_{1,2}$, −40 to −42 cm^{-1} for $[Fe_6-(C_6H_6)_{1,2}]^+$, and −50 to −54 cm^{-1} for $[Fe_6-(C_6H_6)_{1,2}]^-$. The frequency decrease for these two vibrational modes is indicative of a weakening of the bonding in the benzene molecule. Shifted also to the red, the symmetric ring stretching exemplifies clearly a forbidden IR mode of benzene, located at 990 cm^{-1}, that becomes IR active after adsorption; it was found at 962 and 968 cm^{-1} in the monobenzene complexes and at 947 and 953 cm^{-1} in the species containing two benzenes. Furthermore, the in-plane carbon ring distortion and the asymmetric C−H stretching are IR active in benzene; they become IR inactive in $[Fe_6-C_6H_6]^-$ and in $[Fe_6-C_6H_6]^+$, respectively. Then, in this contribution, we addressed the study of the interactions of one and two benzene ligands with the magnetic Fe_6 cluster. This is one of the first studies that deals with this size of iron clusters bonded to benzene. We hope that this research will motivate experimental and theoretical studies on this regime of cluster size, necessary to deeply understand the properties of the $Fe_n-(benzene)_m$ systems.

Acknowledgment. Financial support from Project PAPIIT IN-102308 from DGAPA-UNAM is acknowledged. Supercomputer facilities from DGSCA-UNAM are appreciated. A.G.-G. deeply acknowledges DGAPA-UNAM for his postdoctoral fellowship.

Supporting Information Available: Contour plots for the C−Fe_a bonding MOs of spin down of $Fe_6-(C_6H_6)_2$ are contained in Figure 1 and those, also of spin down, presenting polarization from the axial toward the equatorial iron atoms, and delocalization in the equatorial plane are reported in Figure 2. Some contour plots for the C−Fe_a bonding MOs of majority spin of $Fe_6-C_6H_6$ are reported in Figures 3a,b. The molecular graph for the GS of $Fe_6-C_6H_6$ is contained in Figure 4; there, the density, ρ, in e au^{-3}, and laplacianes, $\nabla^2\rho$, in e au^{-5}, are indicated for the BCPs of the C−Fe and Fe−Fe contacts and the RCPs for the Fe−C−C and Fe−Fe−Fe rings. The contour plots for the HOMO and LUMO orbitals of $Fe_6-C_6H_6$ are reported in Figure 5. This material is available free of charge via the Internet at http://pubs.acs.org.

References and Notes

(1) Bansmann, J.; et al. *Surf. Sci. Rep.* **2005**, *56*, 189.
(2) Billas, I. M. L.; Chatelain, A.; de Heer, W. A. *Science* **1994**, *265*, 1682.
(3) Cox, D. M.; Trevor, D. J.; Whetten, R. L.; Rohlfing, E. A.; Kaldor, A. *Phys. Rev. B* **1985**, *32*, 7290.
(4) Dietz, T. G.; Duncan, M. A.; Powers, D. E.; Smalley, R. *J. Chem. Phys.* **1981**, *74*, 6511.
(5) Duncan, M. A. *Int. J. Mass Spectrom.* **2008**, *272*, 99.
(6) Nakajima, A.; Kaya, K. *J. Phys. Chem. A* **2000**, *104*, 176.
(7) Kurikawa, T.; et al. *Organometallics* **1999**, *18*, 1430.
(8) Senapati, L.; Nayak, S. K.; Rao, B. K.; Jena, P. *J. Chem. Phys.* **2003**, *118*, 8671.

(9) Kandalam, A. K.; Jena, P.; Li, X.; Eustis, S. N.; Bowen, K. H. *J. Chem. Phys.* **2008**, *129*, 134308.
(10) Li, X.; Eustis, S. N.; Bowen, K. H.; Kandalam, A. *J. Chem. Phys.* **2008**, *129*, 124312.
(11) Szczepanski, J.; Wang, H.; Vala, M.; Tielens, A. G. G. M.; Eyler, J. R.; Oomens, J. *ApJ.* **2006**, *646*, 666.
(12) Simon, A.; Joblin, C. *J. Phys. Chem. A* **2007**, *111*, 9745.
(13) Wang, Y.; Szczepanski, J.; Vala, M. *Chem. Phys.* **2007**, *342*, 107.
(14) Simon, A.; Joblin, C.; Polfer, N.; Oomens, J. *J. Phys. Chem. A* **2008**, *112*, 8551.
(15) Hübner, O.; Sauer, J. *Chem. Phys. Lett.* **2002**, *358*, 442.
(16) Rabilloud, F. *J. Chem. Phys.* **2005**, *122*, 134303.
(17) Bauschlicher, C. W.; Partridge, H.; Langhoff, S. R. *J. Phys. Chem.* **1992**, *96*, 3273.
(18) Jaeger, T. D.; van Heijnsbergen, D.; Klippenstein, S. J.; von Helden, G.; Meijer, G.; Duncan, M. A. *J. Am. Chem. Soc.* **2004**, *126*, 10981.
(19) Becke, A. D. *J. Chem. Phys.* **1993**, *98*, 5648–5652.
(20) Stevens, P. J.; Devlin, F. J.; Chablowski, C. F.; Frisch, M. J. *J. Phys. Chem.* **1994**, *98*, 11623.
(21) Becke, A. D. *Phys. Rev. A* **1988**, *38*, 3098.
(22) Perdew, J. P.; Wang, Y. *Phys. Rev.* **1992**, *45*, 13244.
(23) Raghavachari, K.; Trucks, G. W. *J. Chem. Phys.* **1989**, *91*, 1062.
(24) Gutsev, G. L.; Bauschlicher, C. W., Jr. *J. Phys. Chem. A* **2003**, *107*, 7013.
(25) Castro, M. *Chem. Phys. Lett.* **2007**, *435*, 322–326.
(26) Castro, M. *Chem. Phys. Lett.* **2007**, *446*, 333–338.
(27) Valencia, I.; Chávez, V.; Castro, M. *J. Phys. Chem.* **2008**, *112*, 5028.
(28) Kealy, T. J.; Pauson, P. L. *Nature* **1951**, *168*, 1039.
(29) Wilkinson, G.; Rosenblum, M.; Whiting, M. C.; Wooward, R. B. *J. Am. Chem. Soc.* **1952**, *74*, 2125.
(30) Frisch, M. J.; *Gaussian 03*, Revision D.01; Gaussian Inc.: Wallingford, CT, 2004.
(31) Bobadova-Parvanova, P.; Jackson, K. A.; Srinivas, S.; Horoi, M.; Kohler, C.; Seifert, G. *J. Chem. Phys.* **2002**, *116*, 3576.
(32) Castro, M. *Int. J. Quantum Chem.* **1997**, *64*, 223.
(33) Yand, S.; Knickelbein, M. B. *J. Chem. Phys.* **1990**, *93*, 1533.
(34) Wang, L.-S.; Li, X.; Zhang, H.-F. *Chem. Phys.* **2000**, *262*, 53.
(35) (a) Moore, C. E. *Analysis of Optical Spectra*, NSRDS-NBS 34, National Bureau of Standards; National Bureau of Standards: Washington, D.C., 1971. (b) Weast, R. C. *Handbook of Chemistry and Physics*; CRC Press: Boca Raton, FL, 1980; Vol. 61, p E-69. (c) Robinson, J. W. *Handbook of Spectroscopy*; CRC Press: Boca Raton, FL, 1974, Vol. 1, p 257.
(36) Zheng, W.; Eustis, S. N.; Li, X.; Nilles, J. M.; Thomas, O. C.; Bowen, K. H.; Kandalam, A. K. *Chem. Phys. Lett.* **2008**, *462*, 35.
(37) Knickelbein, M. B. *J. Chem. Phys.* **2006**, *125*, 044308.
(38) Dunitz, J. D.; Orgel, L. E.; Rich, A. *Acta Crystallogr.* **1956**, *9*, 373.
(39) Bader, R. F. W. *Atoms in Molecules. A Quantum Theory*; Oxford University Press: New York, NY, 1990.
(40) *AIM2000*; designed by Friedrich Biegler-König; University of Applied Sciences: Bielefeld, Germany, 2000.
(41) Popelier, P. *Atoms in Molecules. An Introduction*, 1st ed.; Prentice-Hall, Pearson Education Limited: Edinburgh Gate, Essex, England, 2000.
(42) Mayer, F.; Khan, I. A.; Armentrout, P. B. *J. Am. Chem. Soc.* **1995**, *117*, 9740.
(43) Pandey, R; Rao, B. K.; Jena, P.; Newsam, J. M. *Chem. Phys. Lett.* **2000**, *321*, 142.
(44) Sun, X.; et al. *J. Appl. Phys.* **2007**, *101*, 09G256.
(45) Pandey, R.; Rao, B. K.; Jena, P.; Blanco, M. A. *J. Am. Chem. Soc.* **2001**, *123*, 3799.
(46) Shimanouchi, T. In *Molecular Vibrational Frequencies, NIST Chemistry WebBook, NIST Standard Reference Database Number 69*; Linstrom, P. J., Mallard, W. G., Eds.; National Institute of Standards and Technology: Gaithersburg, MD, 2007; http:webbook.nist.gov.

JP811065W